transcription. This analysis identified seven novel *mcp* genes (Saito et al., 2004): *mcp1*$^+$ (AB189991); *mcp2*$^+$ (AB189990); *mcp3*$^+$ (AB189989); *mcp4*$^+$ (AB189988); *mcp5*$^+$ (AB189987); *mcp6*$^+$ (AB189986); *mcp7*$^+$ (AB189985).

Mcp6 consists of 327 amino acids and harbours two putative coiled-coil motifs, a leucine zipper (LZ), a nuclear localization signal (NLS), a peroxisomal targeting signal (PTS) and four potential Rad3-kinase phosphorylation target sites (SQ/TQ motifs) (Fig. 1A). Homology searches using the BLAST algorithm (at http://www.ncbi.nlm.nih.gov/BLAST/) indicate that Mcp6 is specific to *S. pombe*, because orthologues were not found in other organisms. Homology searching using the Block Maker program (http://bioinformatics.weizmann.ac.il/blocks/blockmkr/www/make_blocks.html) revealed that not only the coiled-coil domains but also other regions (depicted by filled vertical arrowheads) of Mcp6 are partly homologous to the myosin heavy chain (MHC), which is essential for cytokinesis (Rajagopalan et al., 2003) (Fig. 1B). Partial homology was also found with the SMC family of proteins, which are core components of the cohesin and condensin complexes that are required for chromosome movement (Jessberger, 2002). Moreover, we detected homology to Uso1, a protein required for endoplasmic-reticulum-to-Golgi vesicular transport in *Saccharomyces cerevisiae* (Sapperstein et al., 1996). A common functional feature of these proteins is their involvement in the dynamic movement of subcellular components. This suggests that Mcp6 might also be involved in subcellular dynamics.

The *mcp6*$^+$ gene is meiosis specific and expressed at the horsetail phase

To examine the meiosis-specific transcription of *mcp6*$^+$, we performed northern blot analyses of RNA obtained from CD16-1 (h^+/h^-) and CD16-5 (h^-/h^-) cells harvested at various times after the induction of meiosis by nitrogen starvation. In this experiment, we took advantage of the fact that the heterozygous CD16-1 strain initiates meiosis upon nitrogen starvation, whereas the homozygous CD16-5 strain does not. This analysis revealed that *mcp6*$^+$ displays meiosis-specific transcription that peaks at the horsetail phase (6 hours after induction), which is when homologous chromosome pairing and recombination occur (Fig. 1C).

When the Mcp6 protein appears during meiosis was then assessed by western blot analysis. To attain synchronous meiosis, we used the *pat1-114* temperature-sensitive strain, which enters meiosis in a highly synchronous manner when it is shifted to the restrictive temperature (Iino and Yamamoto, 1985). Thus, *pat1-114 mcp6*$^+$*-gfp* diploid cells that express Mcp6 protein tagged with GFP were induced to enter synchronized meiosis and their lysates were subjected to western blot analysis with an anti-GFP antibody. As shown in Fig. 1D, the frequency of horsetail nuclei is at a normal level, like the *pat1* control (Fig. 3A). Thus, we judged that the function of Mcp6-GFP is intact in this strain. Mcp6-GFP first appeared at the horsetail phase and its expression peaked at 3.5 hours after nitrogen starvation. This is similar to the timing of the production of Meu13 (Nabeshima et al., 2001). These results indicate that Mcp6 is a meiosis-specific protein that is exclusively expressed at the horsetail phase.

Mcp6 localizes to the SPB

We first examined the subcellular localization of Mcp6 by constructing a Mcp6-GFP-expressing strain in the h^{90} genetic background and inducing it to undergo meiosis by nitrogen starvation. As shown in the fluorescent microscope images in Fig. 2A (top), no GFP signal was detected during mitosis. Upon mating, however, the Mcp6-GFP fusion protein appeared as a dot near the edge of the nucleus during the horsetail period of meiosis (Fig. 2A, rows 2,

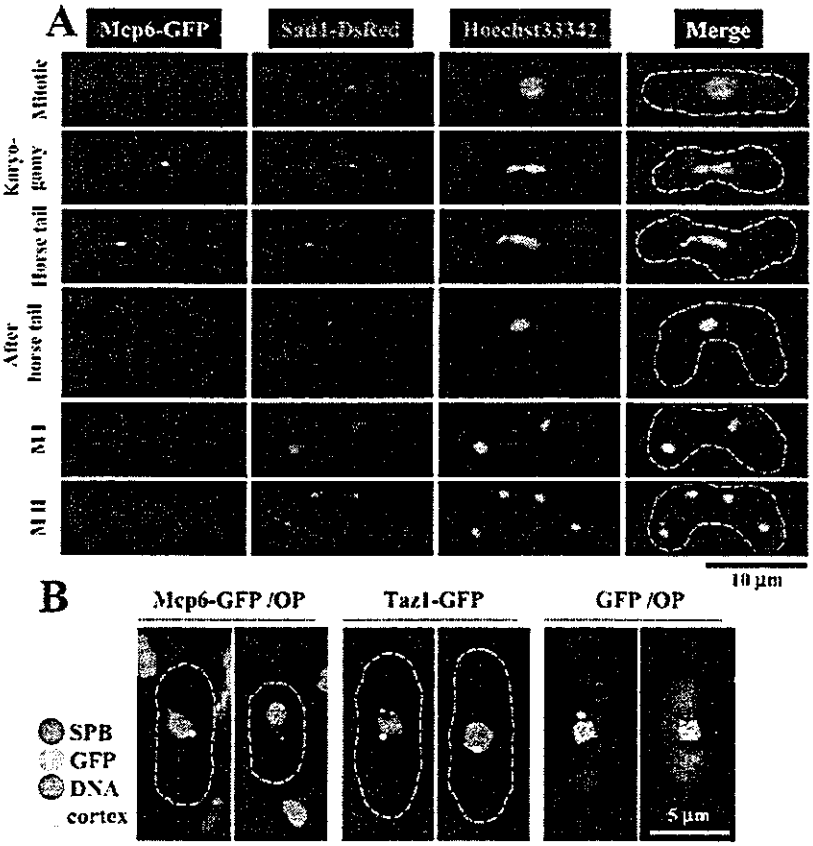

Fig. 2. Mcp6 is a meiosis-specific SPB-associated protein. (A) Microscopic analysis of Mcp6 localization during meiosis. The *mcp6*$^+$*-gfp dsred-sad1*$^+$ strain (ST142) was induced to enter meiosis by nitrogen starvation. After 6 hours of incubation, the cells were collected and fixed with methanol for microscopic observation. The GFP signal is green, the DsRed signal is red and Hoechst 33342 staining is blue. (B) Mcp6-GFP localizes to the SPB but not to the telomeres in mitotic cells. Overproduction by transforming mitotic cells with the pRGT81 (GFP expression vector) or *mcp6*$^+$/pRGT81 (Mcp6-GFP expression vector) plasmid is indicated by 'OP'.

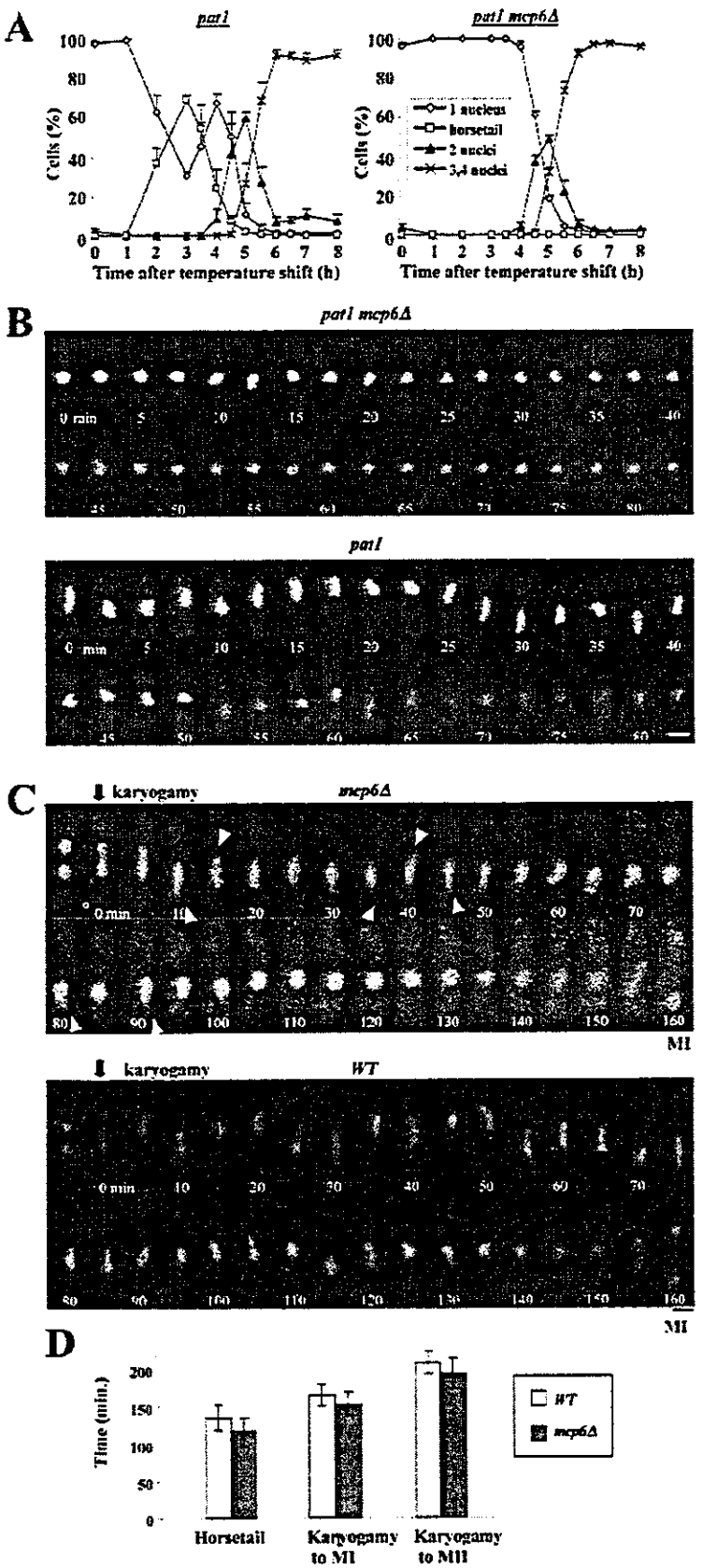

3). The dot disappeared after the horsetail period and the signal was not detected at meiosis I (MI) or meiosis II (MII). The dot localized with the fluorescence signal of Sad1-DsRed, which is known to localize to the SPB (Fig. 2A). Thus, Mcp6 is expressed only during the horsetail period of meiosis and might localize to the SPB.

Because the SPB and telomeres colocalize at this stage of meiosis, it was not clear whether Mcp6 localizes to the SPB or the telomeres. Thus, we expressed Mcp6-GFP (from the *nmt1* promoter in an expression vector pRGT81) and Sad1-DsRed (from the native promoter of *sad1*$^{+}$) during mitotic growth, which is when the SPB and telomeres localize to distinct subcellular loci. We confirmed that Sad1-DsRed does not localize with GFP-tagged Taz1, a component of telomeres, during mitosis (Fig. 2B). However, all of the Mcp6-GFP and Sad1-DsRed colocalized to the edge of the nucleus of the mitotic cells (Fig. 2B), which is where the SPB is known to be located. These results indicate that Mcp6 localizes to the SPB.

Nuclear movement during the meiotic prophase is hampered in the *mcp6Δ* mutant

To determine the role that Mcp6 plays in meiosis, we first examined the meiotic progression of *mcp6Δ* cells. To attain synchronous meiosis, we used the *pat1-114* temperature-sensitive strain again. Thus, homozygous

Fig. 3. Nuclear movement is abnormal during the horsetail phase in *mcp6Δ* cells. (A) Profiles of the meiotic progression in *pat1* (JZ670) and *pat1 mcp6Δ* (TT405) diploid cells (azygotic meiosis). The progression of meiosis was monitored every 30 minutes (3-7 hours) or 1 hour (0-2 hours and 7-8 hours) after the temperature shift, depending on the phase of meiosis. At least 200 cells were counted under a microscope to assess the frequencies of Hoechst-33342-stained cells that bear a horsetail, one nucleus, two nuclei and more than three nuclei. Each point denotes the average value of at least three independent experiments. Standard deviations are indicated as error bars. (B) Time-lapse images of *pat1* and *pat1 mcp6Δ* diploid cells during meiosis I. The nuclei were stained with Hoechst 33342. Images of a single cell were obtained at 2.5-minute intervals. The numbers at the bottom of each photograph represent the timing in minutes, with 0 minute being 2 hours after temperature shift to induce azygotic meiosis. Bar, 5 μm. (C) Time-lapse observation of wild-type (WT) (CT026-1) and *mcp6Δ* (ST193) cells during meiosis I. The nuclei were visualized by the fluorescence of a Polα-GFP fusion construct. Images of a single cell were obtained at 5 minute intervals. The numbers at the bottom of each photograph represent the timing in minutes, with 0 minutes being when nuclear fusion (karyogamy) occurs. The white arrowheads indicate the putative trailing edge of the moving nucleus. Bar, 5 μm. (D) The duration of meiotic prophase, meiosis I (MI) and meiosis II (MII) in *mcp6Δ* and WT cells. The average values were calculated from ten independent cells observed under a microscope. Standard deviations are shown as error bars.

diploid *pat1-114* cells were arrested at the G_1 phase by nitrogen starvation and then shifted to the restrictive temperature to induce synchronous meiosis. We then observed over time the number of nuclei in the cells of the *pat1-114* strain, whose *mcp6*$^+$ gene is intact, and in the cells of the *pat1-114 mcp6Δ* mutant. We found that the times at which cells with two or four nuclei peaked were similar for both strains (Fig. 3A).

Notably, almost no *pat1-114 mcp6Δ* cells (<0.5%) displayed the flat nuclear shape or the non-central position of the nucleus that are characteristic of the horsetail period. This is reminiscent of the description of the cells that bear a mutation in the SBP component Kms1 – that the nuclear shapes of these cells at prophase I of meiosis were aberrant (Shimanuki et al., 1997). Because the oscillatory nuclear movement that normally occurs during the prophase in wild-type meiosis (Chikashige et al., 1994) is impaired in the *kms1-null* mutant (Niwa et al., 2000), we surmised that deletion of *mcp6*$^+$ would also abolish nuclear migration. Thus, we examined over time the movement of chromosomes in *pat1-114 mcp6Δ* cells under a microscope. We found that horsetail oscillation at the prophase of meiosis I was indeed abrogated in these cells (Fig. 3B, top). In fact, almost no nuclear movement was observed throughout the prophase of meiosis in any of the *pat1-114 mcp6Δ* cells that we examined. By contrast, *pat1-114* cells displayed the marked nuclear oscillations that characterize this meiotic period (Fig. 3B, bottom).

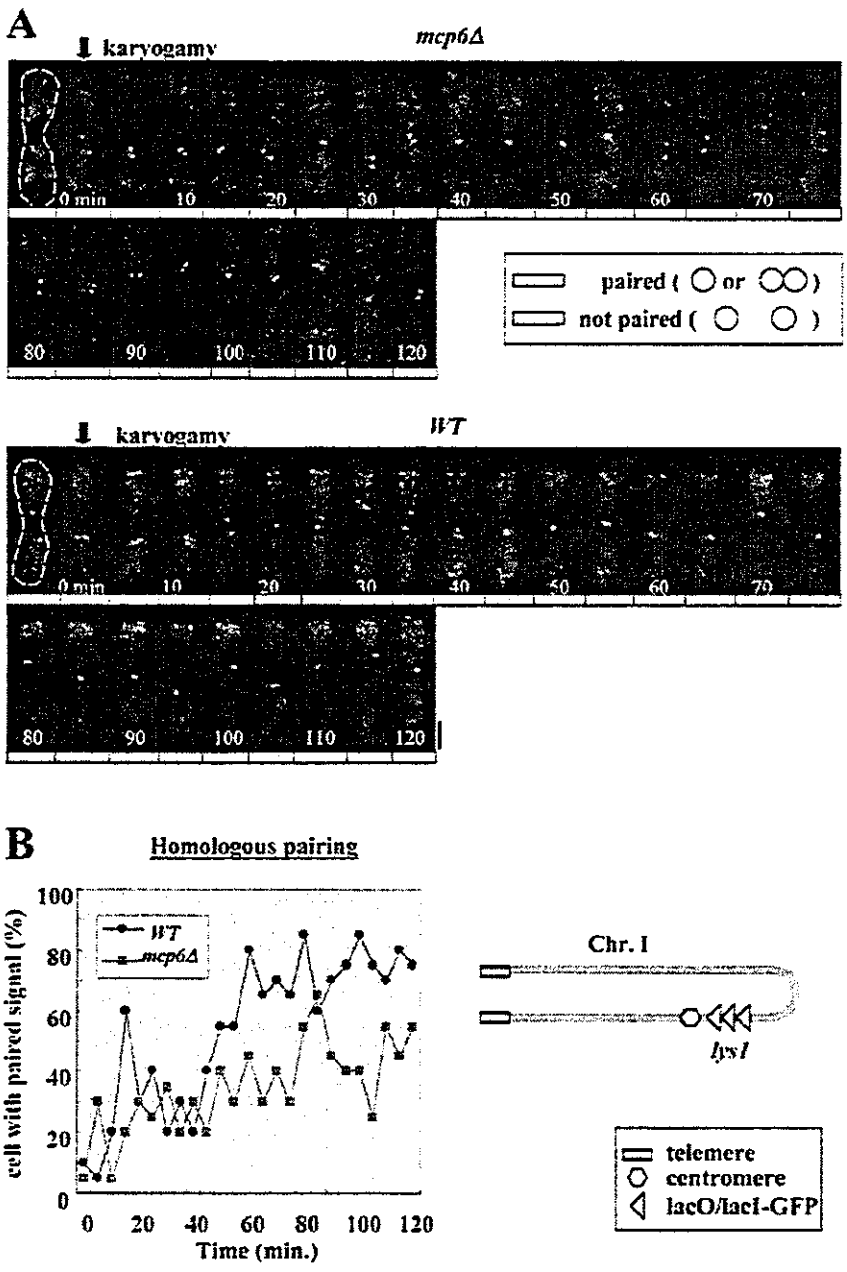

Fig. 4. Homologous pairing is reduced in *mcp6Δ* cells. (A) Time-lapse observation of the *lys1* locus in a living cell, either *mcp6Δ* (ST197) or wild type (WT) (AY174-7B), during the horsetail stage. The *lacO* repeat sequence integrated into the *lys1* loci was visualized by the LacI-NLS-GFP fusion protein. Images of a single cell were obtained at 5 minute intervals. The numbers at the bottom of each photograph represent the timing in minutes, with 0 minutes being when nuclear fusion (karyogamy) occurs. The rectangles under each photo indicate that the *lys1* loci were paired (grey) or not paired (white). Bar, 5 μm. (B) Time course of homologous pairing frequency during the horsetail stage in *mcp6Δ* (red square) compared with that in the WT (blue circle). The average values were calculated from 20 independent cells. The *lys1* locus in chromosome I is illustrated as an inset.

Because the effects of mating and karyogamy cannot be observed at the restrictive temperature in the azygotic meiosis of *h*$^-$/*h*$^-$ *pat1-114* homozygous diploid cells, we also assessed the effect on nuclear oscillation of deleting the *mcp6*$^+$ gene in the *h*^{90} genetic background. Thus, we subjected these cells expressing Polα-GFP to time-lapse observation under a microscope. As shown in Fig. 3C (top), it is apparent that nuclear oscillation at prophase of meiosis I is also impaired in *mcp6Δ* cells. Notably, in contrast to *pat1-114 mcp6Δ* cells, slight movement was observed just after karyogamy, although no apparent movement was detected thereafter. The nucleus does seem to be moving a little in *mcp6Δ* cells because a trace of the trailing edge of the moving nucleus can be observed (Fig. 3B, white arrowheads). Nonetheless, it is evident that chromosomal movement is largely hampered in *mcp6Δ* cells compared with the vigorous nuclear movements in wild-type cells that occur several times after karyogamy (Fig. 3C, bottom).

Although it seems that the horsetail period (117 minutes) and the periods from karyogamy to meiosis I (154 minutes) and from karyogamy to meiosis II (195 minutes) in *mcp6Δ* cells were slightly shorter than those of wild-type cells (136 minutes, 166 minutes and 209 minutes, respectively) (Fig. 3D), these changes were not statistically

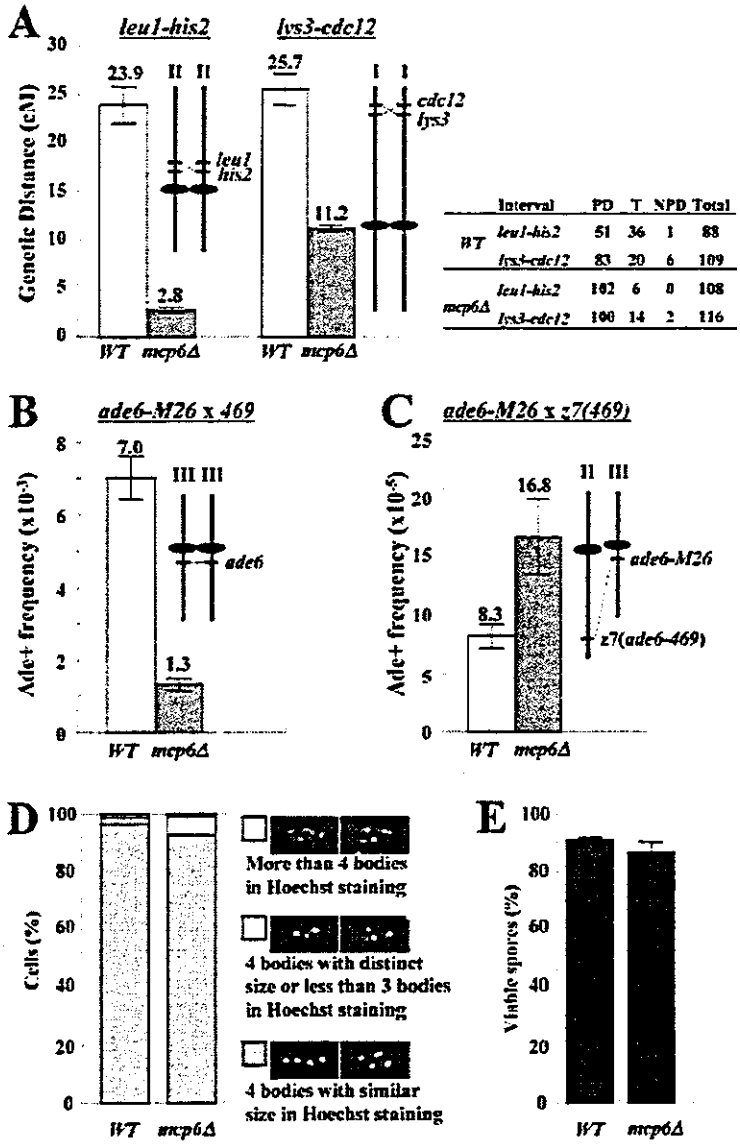

Fig. 5. Homologous recombination is reduced in *mcp6Δ* cells but ectopic recombination is increased compared with wild-type (WT) cells. The chromosomal positions of the loci and centromeres are illustrated in the insets. (A) Intergenic recombination (crossing over) showing the intervals between *leu1* and *his2* (left), *lys3* and *cdc12* (middle) and the primary tetrad (right). Only those tetrads that generated four viable spores were used to calculate the genetic distances (cM). The strains examined for *leu1-his2* crossing were WT (TT8-1 × NP32-2A) and *mcp6Δ* (TT398 × TT399), whereas the strains used for the *lys3-cdc12* crossing were WT (TT8-1 × TT231-1) and *mcp6Δ* (TT399 × TT411). The data shown are the average values calculated from at least three independent assays (at least 40 tetrads were dissected per assay). (B) Intragenic recombination. The strains examined were WT (MS105-1B × MS111w1) and *mcp6Δ* (TT400 × TT401). The average values were calculated from at least three independent assays. (C) Ectopic intragenic recombination. The strains crossed were WT (MS105-1B × GP1123) and *mcp6Δ* (TT400 × TT1014). The average values were calculated from at least three independent assays. Standard deviations are indicated as error bars. (D) Spores of *mcp6Δ* cells are almost normal as judged by the frequency of abnormal ascospores. The haploid parental strains were mated and sporulated on ME plate. After overnight culture, the cells were fixed with 70% ethanol for staining with Hoechst 33342. At least 200 cells were counted. (E) Spore viability of WT (TP4-5A × TP4-1D) and *mcp6Δ* (TT397-5A × TT397-1D) cells. Random spore analysis was performed.

significant ($P>0.05$ in Student's *t*-test). Thus, we conclude that the durations of the horsetail period, meiosis I and meiosis II are almost normal in h^{90} *mcp6Δ* cells (zygotic meiosis), as they are in the *pat1-114* genetic background (azygotic meiosis).

Homologous pairing is reduced in *mcp6Δ* cells

To investigate the requirement of Mcp6 in the process of chromosome pairing, we observed the homologous chromosomal regions in living zygotes during horsetail phase. By integrating a tandem repeat of the *Escherichia coli lac* operator sequence into the *S. pombe* genome at the *lys1*$^+$ locus (near the centromere of chromosome I), the fusion gene encoding GFP-LacI-NLS (which binds to the *lac* operator) was expressed in this strain. Consequently, two homologous loci on the chromosomes were visualized with GFP fluorescence (Nabeshima et al., 2001). In wild-type background, these homologous loci repeatedly associated and dissociated in the horsetail nucleus, oscillating back and forth between the cell poles (Fig. 4A, bottom). By contrast, the paired GFP signals were less frequent in *mcp6Δ* cells than in wild-type cells (Fig. 4A, top).

In order to quantify the pairing activity during the horsetail phase, we scored the occurrence of paired signals every 5 minutes from karyogamy to the first meiotic nuclear division in 20 live individuals of each strain. In the wild-type strain, the population of cells with paired signals during the initial 45 minutes was about 30% and then increased to about 80%. This level was maintained until 120 minutes (Fig. 4B, blue line). In *mcp6Δ* cells, there was no significant difference from the wild type in the initial 45 minutes but the subsequent increase in pairing observed in the wild type was completely absent (Fig. 4B, red line). These results indicate that Mcp6 is required for promoting homologous pairing with horsetail movement.

Meiotic recombination is abnormal in *mcp6Δ* cells

To determine whether, like the other SPB component Kms1, Mcp6 plays a role in meiotic recombination (Niwa et al., 2000), we compared the rates of intergenic and intragenic recombination in *mcp6Δ* and wild-type strains. We first investigated the crossover recombination of zygotic meiosis by tetrad analysis, which allowed us to measure the genetic distance between *leu1* and *his2* (Fig. 5A, insets). When the *mcp6Δ* strain was crossed, the genetic distance between *leu1* and *his2* was only 12% of the distance obtained when the wild-type strain was crossed (Fig. 5A, left). The genetic distances

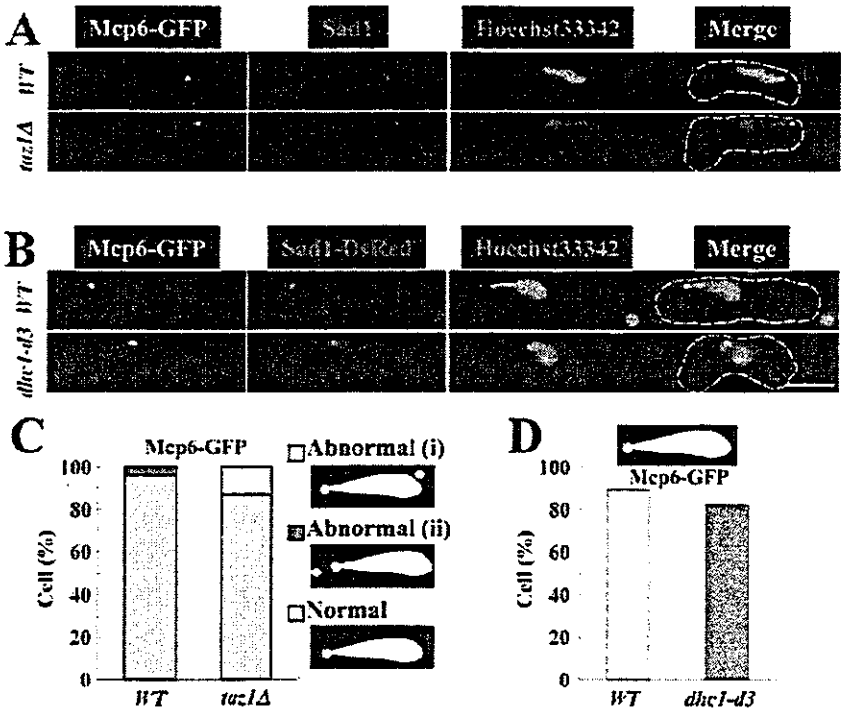

Fig. 6. The localization of Mcp6-GFP is normal in *taz1Δ* and *dhc1-d3* cells. (A) A typical immunofluorescence image of Mcp6-GFP at the horsetail phase in wild type (ST134) and *taz1Δ* (ST200) cells. (B) A typical image of Mcp6-GFP at the horsetail phase in wild-type (ST142) and *dhc1-d3* (ST196) cells (living). Bar, 5 μm. (C) Frequency of cells in which the Mcp6-GFP signals localize with Sad1 to the leading edge of the horsetail nucleus in the wild type and *taz1Δ* cells. (D) Frequency of cells in which the Mcp6-GFP signals localize with Sad1-DsRed to the leading edge of the horsetail nucleus in the wild-type and *dhc1-d3* cells.

between *lys3* and *cdc12* in the *mcp6Δ* strain was also reduced to 44% of that observed in the wild-type strain (Fig. 5A, right). We also characterized the intragenic recombination of the *mcp6Δ* strain between two different mutant alleles of *ade6* (*M26* and *469*). When the *mcp6Δ* strain was crossed, the frequency of Ade$^+$ recombinant spores was 19% of the wild-type frequency (Fig. 5B). Thus, it appears that Mcp6 plays a significant role in meiotic recombination.

To characterize the meiotic recombination competency of the *mcp6Δ* strain further, we examined the ectopic recombination rate. We used a pair of *ade6* alleles from different chromosomal loci, one at the natural position of *ade6* on chromosome III and the other at the *pac1* locus on chromosome II (*z7*) (Virgin and Bailey, 1998) (Fig. 5C). Notably, the frequency of ectopic recombination between these two loci in *mcp6Δ* cells was twice (202%) (in the *M26* and *469* pair) that of wild-type cells (Fig. 5C). A similar increase in the ectopic recombination rate between *M26* and *z15* (telomere of chromosome I) has been reported for the *kms1Δ* strain (Niwa et al., 2000). However, *mcp6Δ* cells are distinct from *kms1Δ* cells in that they do not display the abnormal telomere clustering that characterizes *kms1Δ* cells.

When we observed the spore morphology of *mcp6Δ* cells, we found that almost all of the spores looked normal (Fig. 5D). Indeed, depletion of Mcp6 caused only about 4% of the asci to display abnormal numbers of ascospores. The spore viability is also similar to that of wild-type cells (Fig. 5E). Thus, we conclude that Mcp6 does not play an important role in spore formation.

Taz1 and Dhc1 are not required for the localization of Mcp6 at the leading edge of the horsetail nucleus

In addition to chromosome oscillation at the horsetail phase, telomere clustering is required for the alignment and subsequent association of homologous chromosome arms (Ding et al., 2004). The telomere protein Taz1, whose deletion causes G_2/M-phase DNA-damage-checkpoint delay, chromosome mis-segregation and double-stranded DNA breaks, plays a role in preventing and repairing DNA breaks (Miller and Cooper, 2003) and telomere clustering (Cooper et al., 1998). To determine whether the SPB localization of Mcp6 depends on proper telomere clustering, we prepared *taz1* null mutant cells harbouring the integrated *mcp6$^+$-gfp* gene driven by its own promoter. These cells were then induced to enter meiosis by nitrogen starvation and the Mcp6-GFP signal was observed by immunofluorescence. As shown in Fig. 6A,C, the subcellular localization of Mcp6-GFP was almost normal in *taz1Δ* cells (71 cells were counted in both wild-type and *mcp6Δ* cells).

We next examined whether SPB localization of Mcp6 is dependent on dynein. To do this, we prepared a *dhc1-d3* mutant harbouring the integrated *mcp6$^+$-gfp* gene driven by its own promoter and induced it to enter meiosis by nitrogen starvation. Mcp6-GFP colocalized normally with DsRed-Sad1 to the SPB in *dhc1-d3* cells, which suggests that Dhc1 is not required for the proper localization of Mcp6 at the SPB (Fig. 6B). The frequency of cells in which Sad1-DsRed and Mcp6-GFP colocalized to the leading edge of the horsetail nucleus was 94% (15/18) in *dhc1-d3* cells, which is almost equal to the frequency in wild-type cells (93%; 32/36) (Fig. 6D).

Subcellular localization of SPB components is normal in *mcp6Δ* cells

For proper horsetail movement, it is essential that the telomeres cluster at the SPB after karyogamy and that the telomere/SPB complex migrates on the microtubule that radially extends from the SPB to the cell cortex on the opposite site of the cell. To understand the role of Mcp6 in horsetail movement, we examined the subcellular localization of the SPB components Sad1, Spo15 and Kms1 in *mcp6Δ* cells. Sad1 is a constitutive component of SPB that is essential for normal bipolar spindle formation (Hagan and Yanagida, 1995), Spo15 is associated with SPBs throughout the life cycle and plays an indispensable role in the initiation of spore membrane formation (Ikemoto et

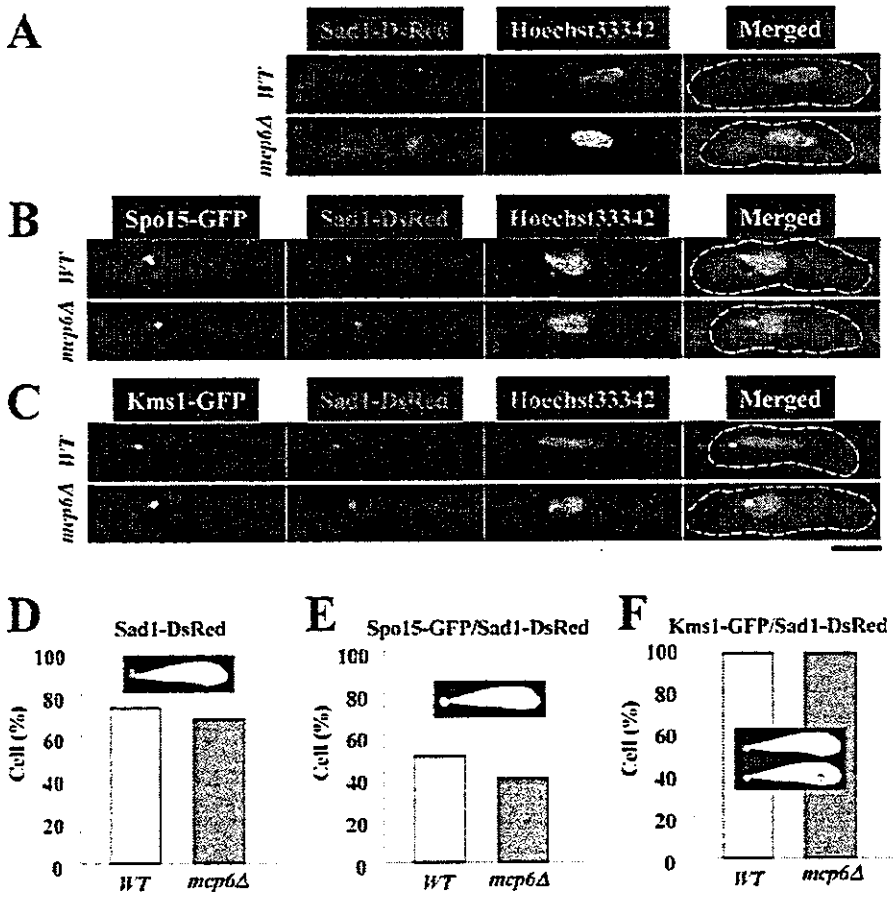

Fig. 7. The subcellular localization of GFP-tagged SPB components at the horsetail phase is normal in *mcp6Δ* cells. The h^{90} strains that express Sad1-DsRed (WT, CRL790; *mcp6Δ*, ST148) (A), Spo15-GFP (*WT*, ST176; *mcp6Δ*, ST171-1) (B) or Kms1-GFP (*WT*, ST191-1; *mcp6Δ*, ST172-1) (C) fusion proteins were induced to enter meiosis by nitrogen starvation. After 6 hours, the cells were collected and observed under a fluorescence microscope. Typical images are shown. (D) The proportions of the cell population in which Sad1-DsRed localized to the leading edge of the nucleus with a single dot, as depicted in the inset. (E) The proportions of the cell population in which Spo15-GFP and Sad1-DsRed colocalized to the leading edge of the nucleus with a single dot, as depicted in the inset. (F) The proportions of the cell population in which Kms1-GFP and Sad1-DsRed colocalized to the leading edge of the nucleus, as depicted in the inset. Green, GFP; red, Sad1-DsRed; blue, Hoechst 33342. The dotted line depicts the contour of the cell. Bar, 5 μm.

al., 2000), and Kms1 is required for the formation of meiotic prophase-specific nuclear architecture (Shimanuki et al., 1997). To do this, we prepared strains that express the Sad1-dsRed protein and the other GFP-fused components from their own promoters in the *mcp6-null* genetic background. The cells were induced to enter meiosis by nitrogen starvation and then observed under a fluorescence microscope.

We first investigated the localization of Sad1-dsRed during the horsetail phase and found that, in *mcp6Δ* cells, 68% (17/25) of the Sad1 signal constituted a single dot at the leading edge of the nucleus (Fig. 7A,D). This is similar to what is observed in wild-type cells (59/82, or 72%, of the Sad1 signal is present as a single dot). These results indicate that Mcp6 is not required for Sad1 localization to the SPB. We next examined the localization of Spo15-GFP and found that most of the Spo15 signal localized with Sad1-DsRed to the SPB in both *mcp6Δ* and wild-type cells (Fig. 7B,E). We also examined the localization of Kms1-GFP and found that most Kms1-GFP and Sad1-DsRed colocalized to either the SPB or the Sad1 body in both *mcp6Δ* and wild-type cells (Fig. 7C,F). These results indicate that Mcp6 is not required for the proper organization of SPB architecture.

Telomere localization is normal but microtubule organization is abnormal in *mcp6Δ* cells

Telomere clustering near the SPB, which occurs during the prophase of meiosis I, is an essential event for efficient chromosome pairing and cells deficient in the telomere-associated protein Taz1 (*taz1Δ*) have been reported to have defective telomere clustering, reduced recombination rates, abnormal spore formation and reduced spore viability (Nimmo et al., 1998; Cooper et al., 1998). To determine whether telomere clustering is normal in *mcp6Δ* cells, we examined the subcellular localization of the telomere proteins Taz1 and Swi6 by preparing h^{90} *taz1⁺-gfp sad1⁺-dsred* and h^{90} *swi6⁺-gfp sad1⁺-dsred* strains, which express Sad1-dsRed together with GFP-tagged Taz1 or Swi6 from their own promoters. These strains were induced to enter meiosis by nitrogen starvation and then observed under a fluorescence microscope. The Taz1-GFP signal of the telomere at the leading edge of the nucleus localized with the Sad1-DsRed signal to the SPB in 62% (23/37) and 58% (14/24) of the *mcp6Δ* and wild-type cells, respectively (Fig. 8A,D). The Swi6-GFP signal also localized with the Sad1-DsRed signal to the SPB at similar levels in *mcp6Δ* (76%; 13/17) and wild-type cells (85%; 35/41) (Fig. 8B). These results indicate that the subcellular localization of Taz1 and Swi6 is normal in *mcp6Δ* cells – namely, Mcp6 is required for neither SPB organization nor telomere clustering.

The oscillatory nuclear movement is mediated by dynamic reorganization of astral microtubules originating from the SPB. To observe the organization of microtubules in *mcp6Δ* cells, we prepared the h^{90} strain that expresses GFP-fused α-tubulin from the *nmt1* promoter. After 6 hours' induction of meiosis

in EMM2-N medium, the strain was fixed with glutaraldehyde and paraformaldehyde for immunostaining. In wild-type cells, 95% (156/165) of astral microtubules originated from the SPB during the horsetail phase. In *mcp6Δ* cells, however, collapse of astral microtubule organization was observed (Fig. 8C,F): 21% (21/100) of *mcp6Δ* cells displayed the microtubules not associated with SPB [Fig. 8F, abnormal (i)]. We also found that 60% (60/100) of *mcp6Δ* cells showed abnormal astral microtubules that originated from the SBP but branched elsewhere [Fig. 8F; abnormal (ii)]. These results indicate that Mcp6 is required for proper astral microtubule positioning during horsetail phase.

Discussion

Mcp6 is required for horsetail movement of chromosomes

In the present study, we show that Mcp6 is a novel coiled-coil protein that is only expressed during the horsetail period of meiosis (Fig. 1) and localizes to the SPB (Fig. 2). We found that the deletion of *mcp6*$^+$ almost abolished horsetail movement of chromosomes (Fig. 3) and reduced recombination rates (Fig. 5). Notably, we observed that, whereas deletion of *mcp6*$^+$ from the homozygous diploid *pat1* genetic background completely abolished horsetail movement during azygotic meiosis of these cells (Fig. 3B), a slight chromosome movement after karyogamy was observed during the zygotic meiosis of *mcp6Δ* cells in the h^{90} genetic background (Fig. 3C). This indicates that karyogamy is important for initiating horsetail movement and suggests that Mcp6 plays a role during or just after karyogamy. BLAST-based homology searches failed to identify proteins in other species that are homologous to Mcp6. Thus, Mcp6 is an *S.-pombe*-specific protein. This is reasonable because *S. pombe* is the only organism examined so far that displays horsetail movement of nucleus.

Two *S. pombe* mutants [*kms1-1* (Shimanuki et al., 1997; Niwa et al., 2000) and *dhc1* mutants (Yamamoto et al., 1999)] have been reported to lack horsetail movement. Another mutant (*dlc1Δ*) also shows abnormal horsetail movement (Miki et al., 2002). Although Kms1, which is also an *S.-pombe*-specific protein, localizes to the SPB throughout mitotic and meiotic phases, abnormal phenotypes of *kms1-1* cells are only detected in meiosis (Niwa et al., 2000). Dhc1, the dynein heavy chain that is conserved among various species, localizes to the SPB, microtubules and cell cortex, and is predominantly expressed from karyogamy through to meiosis I (Yamamoto et al., 1999). Thus, Mcp6 is a new

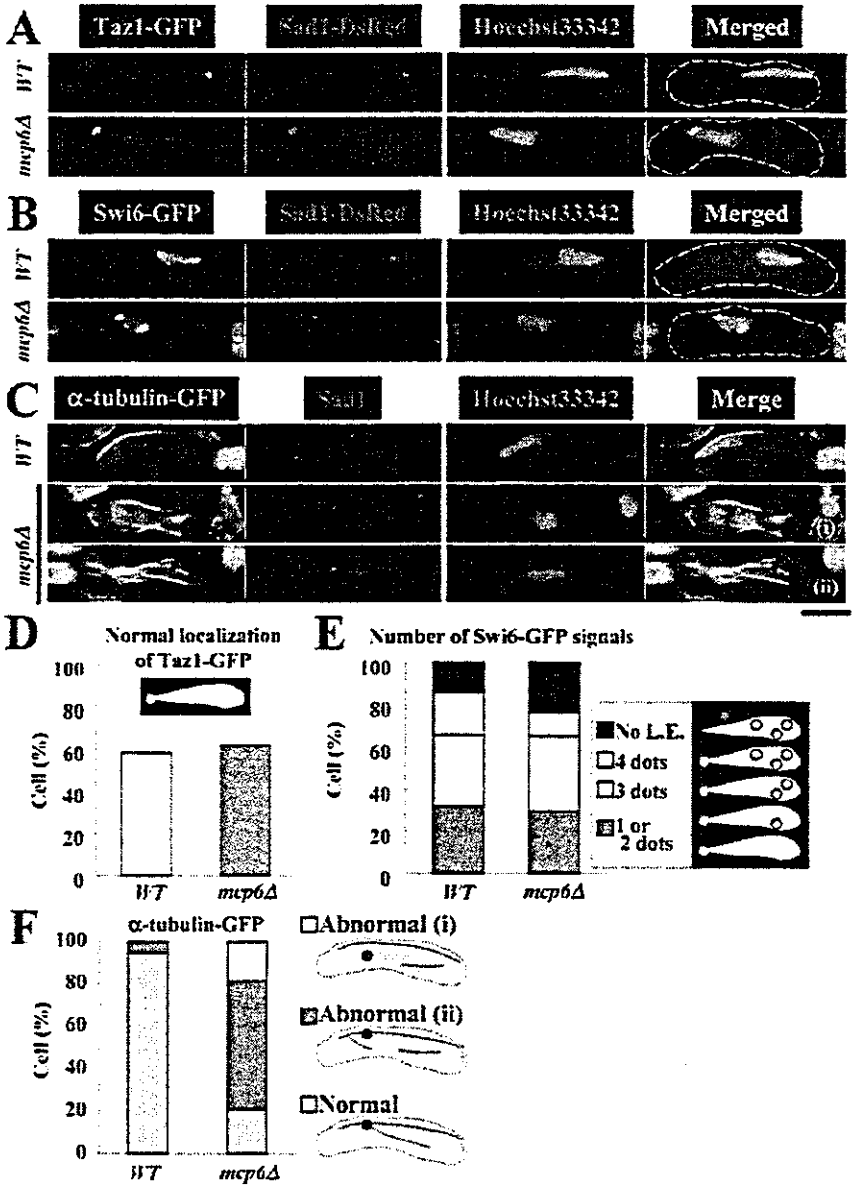

Fig. 8. GFP-tagged telomere components and α-tubulin localize normally in *mcp6Δ* cells. The h^{90} strains that express Taz1-GFP (*WT*, ST178; *mcp6Δ*, ST173) (A), Swi6-GFP (*WT*, ST179-1; *mcp6Δ*, ST174) (B) or α-tubulin-GFP (*WT*, YY105; *mcp6Δ*, ST146) (C) were induced to enter meiosis by nitrogen starvation. After 6 hours, the cells were collected and observed under a fluorescence microscope. Images shown in (C) were obtained by immunofluorescence. Typical images are shown. (D) The proportions of the cell population in which Taz1-GFP and Sad1-DsRed colocalized to the leading edge of the nucleus with a single dot, as depicted in the inset. (E) The proportions of the cell population in which Swi6-GFP and Sad1-DsRed colocalized to the leading edge (L.E.) of the nucleus with extra dots of Swi6-GFP in the nucleus, as depicted in the insets. (F) The proportions of the cell population that display normal or abnormal (i) and (ii) tubulin positioning as depicted on the right. Green, GFP; red, Sad1-DsRed (A,B) or Sad1 (C); blue, Hoechst 33342. The dotted line indicates the contour of the cell. Bar, 5 μm.

member of this group of SPB- and horsetail-movement-associated proteins. In support of this, *mcp6Δ* cells show similar phenotypes to the *kms1-1*, *kms1Δ*, *dhc1* and *dlc1Δ* mutant cells as follows. First, like *kms1*, *dhc1* and *dlc1Δ* mutants, the rates of intergenic or intragenic recombination of the *mcp6Δ* mutant are markedly reduced (Fig. 5A,B). Second, the ectopic recombination rate of *mcp6Δ* cells is increased about twofold (Fig. 5C), as has also been observed for the ectopic recombination of *kms1Δ* cells between *ade6-M26* and *ade6-469* (*z15*) loci, although the rate of ectopic recombination between the *ade6-M26* and *ade6-469* (*z7*) loci in *kms1Δ* cells was almost the same as that in wild-type cells (Niwa et al., 2000).

However, Mcp6 does have some phenotypes that differ from those of *kms1*, *dhc1* and *dlc1Δ* mutants, and thus it seems to play a distinct role in maintaining the horsetail movement. One such phenotype is the almost normal spore formation and spore viability in *mcp6Δ* cells (Fig. 5D,E). By contrast, spore formation and spore viability are abnormal in *kms1Δ*, *dhc1Δ* and *dlc1Δ* cells. Second, unlike *kms1Δ* cells (Shimanuki et al., 1997), telomere clustering, as determined by examining the subcellular localization of Taz1-GFP and Swi6-GFP, appears almost normal in *mcp6Δ* cells (Fig. 8). Third, although *kms1Δ* and *dhc1-d3* cells showed reduced SPB integrity and abnormal chromosome segregation, respectively, the *mcp6Δ* mutant does not show such abnormalities (Figs 6, 7). Fourth, Mcp6 is the only meiosis-specific protein of this group, because Kms1, Dhc1 and Dlc1 are also detected in both the mitotic and meiotic phases (Goto et al., 2001; Miki et al., 2002).

Mcp6 plays a role in homologous pairing by regulating horsetail movement

We report here that recombination rates are greatly reduced in *mcp6Δ* cells compared with wild-type cells (Fig. 5), which is due primarily to the inefficient homologous pairing of chromosomes in *mcp6Δ* cells (Fig. 4). This inefficient homologous pairing is mainly derived from the impaired horsetail movement of nucleus (Fig. 3). We previously showed that *meu13Δ* and *mcp7Δ* cells show a delay in entering meiosis I, and that this is due to the meiotic recombination checkpoint that provides cells with enough time to repair double-strand breaks (DSBs) in a manner dependent on checkpoint *rad*$^+$ genes (Shimada et al., 2002; Saito et al., 2004). In the case of *mcp6Δ* cells, however, even though recombination rates were reduced, a delay in entering meiosis I was not observed (Fig. 3A). Thus, we surmise that Mcp6 is not involved in DSB repair like other SPB components, probably because Mcp6 is located at the SPB, a location that is too remote directly to regulate DSBs on chromatin. Similarly, Mcp6 might not directly regulate the recombination machinery. Thus, it is most probable that Mcp6 is involved in regulating the pairing of homologous chromosomes by inducing proper horsetail movement.

Mcp6 is a novel type of regulator of horsetail movement

Some mutants (*lot2-s17*, *lot3-uv3/taz1*, *dot1* and *dot2*) show defective horsetail movement and reduced meiotic recombinations, but their phenotypes are distinct from *mcp6Δ*. For example, *lot2-s17* and *lot3-uv3/taz1* mutants display a dramatic lengthening of telomeric repeats, low spore viability and chromosome mis-segregation through meiosis (Nimmo et al., 1998; Cooper et al., 1998; Hiraoka et al., 2000). Two mutants (*dot1* and *dot2*) do not sporulate and show defective SPB integrity and impaired telomere clustering (Jin et al., 2002). By contrast, we show here that *mcp6Δ* differs from these mutants because sporulation (Fig. 5D,E), SPB integrity (Fig. 7) and telomere clustering (Fig. 6) are almost normal.

Some mutant strains of *taz1* that show abnormal horsetail movement (Hiraoka et al., 2000) are also distinct from *mcp6Δ* cells. First, telomere clustering is abnormal in *taz1Δ* cells. Second, *taz1Δ* cells display abnormal spore formation and reduced spore viability. Third, although the subcellular localization of Taz1-GFP is normal in *mcp6Δ* cells (Fig. 8A), Mcp6-GFP localization became slightly abnormal in *taz1Δ* cells (Fig. 6A,C). Thus, Mcp6 might interact with Taz1 but its role in chromosome maintenance during meiosis is quite distinct.

Finally, microtubules are nucleated exclusively from SPBs immediately after karyogamy and form typical X-shaped configurations during nuclear fusion of meiotic cells (Svoboda et al., 1995; Yamamoto et al., 1999). However, we report here that the astral microtubule organization was largely abnormal in *mcp6Δ* cells (Fig. 8). Thus, in the absence of Mcp6, many cells fail to organize a long, curved microtubule array that extends from the cell ends to provide the tracks for nuclear horsetail movement, resulting in the abolished nuclear oscillation and reduced chromosome pairing. Taken together, we conclude that Mcp6 controls horsetail movement by regulating the astral microtubule organization during meiosis.

We thank O. Niwa, Y. Hiraoka, A. Yamamoto, C. Shimoda, M. Yamamoto, G. R. Smith, K. M. Miller and W. Z. Cande for providing *S. pombe* strains, and O. Niwa for the anti Sad1 antibody. We also thank K. Nabeshima for technical advice in the experiments of chromosome pairing, E. Okamura for technical assistance, and P. Hughes for critically reading the manuscript. This work was supported by a Grant-in-aid for Scientific Research on Priority Areas from the Ministry of Education, Science, Sports and Culture of Japan and a grant from the Uehara Memorial Foundation to H.N.

References

Alfa, C., Fantes, P., Hyams, J., McLeod, M. and Warbrick, E. (1993). *Experiments with Fission Yeast: A laboratory course manual.* Cold Spring Harbor Laboratory Press, Cold Spring Harbor, NY, USA.

Burkhard, P., Stetefeld, J. and Strelkov, S. V. (2001). Coiled coils: a highly versatile protein folding motif. *Trends Cell Biol.* **11**, 82-88.

Chikashige, Y., Ding, D. Q., Funabiki, H., Haraguchi, T., Mashiko, S., Yanagida, M. and Hiraoka, Y. (1994). Telomere-led premeiotic chromosome movement in fission yeast. *Science* **264**, 270-273.

Chikashige, Y., Ding, D. Q., Imai, Y., Yamamoto, M., Haraguchi, T. and Hiraoka, Y. (1997). Meiotic nuclear reorganization: switching the position of centromeres and telomeres in the fission yeast *Schizosaccharomyces pombe*. *EMBO J.* **16**, 193-202.

Cooper, J. P., Watanabe, Y. and Nurse, P. (1998). Fission yeast Taz1 protein is required for meiotic telomere clustering and recombination. *Nature* **392**, 828-831.

Ding, D. Q., Chikashige, Y., Haraguchi, T. and Hiraoka, Y. (1998). Oscillatory nuclear movement in fission yeast meiotic prophase is driven by astral microtubules, as revealed by continuous observation of chromosomes and microtubules in living cells. *J. Cell Sci.* **111**, 701-712.

Ding, D. Q., Tomita, Y., Yamamoto, A., Chikashige, Y., Haraguchi, T. and Hiraoka, Y. (2000). Large-scale screening of intracellular protein localization in living fission yeast cells by the use of a GFP-fusion genomic DNA library. *Genes Cells* **5**, 169-190.

Ding, D. Q., Yamamoto, A., Haraguchi, T. and Hiraoka, Y. (2004). Dynamics of homologous chromosome pairing during meiotic prophase in fission yeast. *Dev. Cell* **6**, 329-341.

Fukushima, K., Tanaka, Y., Nabeshima, K., Yoneki, T., Tougan, T., Tanaka, S. and Nojima, H. (2000). Dmc1 of *Schizosaccharomyces pombe* plays a role in meiotic recombination. *Nucleic Acids Res.* **28**, 2709-2716.

Goto, B., Okazaki, K. and Niwa, O. (2001). Cytoplasmic microtubular system implicated in de novo formation of a Rabl-like orientation of chromosomes in fission yeast. *J. Cell Sci.* **114**, 2427-2435.

Grimm, C., Kohli, J., Murray, J. and Maundrell, K. (1988). Genetic engineering of *Schizosaccharomyces pombe*: a system for gene disruption and replacement using the ura4 gene as a selectable marker. *Mol. Gen. Genet.* **215**, 81-86.

Gutz, H. (1971). Gene conversion: remarks on the quantitative implications of hybrid DNA models. *Genet. Res.* **17**, 45-52.

Hagan, I. and Hyams, S. J. (1988). The use of cell division cycle mutants to investigate the control of microtubule distribution in the fission yeast *Schizosaccharomyces pombe*. *J. Cell Sci.* **89**, 343-357.

Hagan, I. and Yanagida, M. (1995). The product of the spindle formation gene *sad1*$^{+}$ associates with the fission yeast spindle pole body and is essential for viability. *J. Cell Biol.* **129**, 1033-1047.

Hiraoka, Y. (1998). Meiotic telomeres: a matchmaker for homologous chromosomes. *Genes Cells* **3**, 405-413.

Hiraoka, Y., Ding, D. Q., Yamamoto, A., Tsutsumi, C. and Chikashige, Y. (2000). Characterization of fission yeast meiotic mutants based on live observation of meiotic prophase nuclear movement. *Chromosoma* **109**, 103-109.

Ikemoto, S., Nakamura, T., Kubo, M. and Shimoda, C. (2000). *S. pombe* sporulation-specific coiled-coil protein Spo15p is localized to the spindle pole body and essential for its modification. *J. Cell Sci.* **113**, 545-554.

Iino, Y. and Yamamoto, M. (1985). Mutants of *Schizosaccharomyces pombe* which sporulate in the haploid state. *Mol. Gen. Genet.* **198**, 416-421.

Jin, Y., Uzawa, S. and Cande, W. Z. (2002). Fission yeast mutants affecting telomere clustering and meiosis-specific spindle pole body integrity. *Genetics* **160**, 861-876.

Jessberger, R. (2002). The many functions of SMC proteins in chromosome dynamics. *Nat. Rev. Mol. Cell Biol.* **10**, 767-778.

Kanoh, J. and Ishikawa, F. (2001). spRap1 and spRif1, recruited to telomeres by Taz1, are essential for telomere function in fission yeast. *Curr. Biol.* **11**, 1624-1630.

Kohli, J. (1994). Meiosis. Telomeres lead chromosome movement. *Curr. Biol.* **4**, 724-727.

Loidl, J. (1990). The initiation of meiotic chromosome pairing: the cytological view. *Genome* **33**, 759-778.

Miki, F., Okazaki, K., Shimanuki, M., Yamamoto, A., Hiraoka, Y. and Niwa, O. (2002). The 14-kDa dynein light chain-family protein Dlc1 is required for regular oscillatory nuclear movement and efficient recombination during meiotic prophase in fission yeast. *Mol. Biol. Cell* **13**, 930-946.

Miller, K. M. and Cooper, J. P. (2003). The telomere protein Taz1 is required to prevent and repair genomic DNA breaks. *Mol. Cell* **11**, 303-313.

Nabeshima, K., Kakihara, Y., Hiraoka, Y. and Nojima, H. (2001). A novel meiosis-specific protein of fission yeast, Meu13p, promotes homologous pairing independently of homologous recombination. *EMBO J.* **20**, 3871-3881.

Nimmo, E. R., Pidoux, A. L., Perry, P. E. and Allshire, R. C. (1998). Defective meiosis in telomere-silencing mutants of *Schizosaccharomyces pombe*. *Nature* **392**, 825-828.

Niwa, O., Shimanuki, M. and Miki, F. (2000). Telomere-led bouquet formation facilitates homologous chromosome pairing and restricts ectopic interaction in fission yeast meiosis. *EMBO J.* **19**, 3831-3840.

Okuzaki, D., Satake, W., Hirata, A. and Nojima, H. (2003). Fission yeast *meu14*$^{+}$ is required for proper nuclear division and accurate forespore membrane formation during meiosis II. *J. Cell Sci.* **116**, 2721-2735.

Perkins, D. D. (1949). Biochemical mutants in smut fungus *Ustilago maydis*. *Genetics* 34, 607-626.

Rajagopalan, S., Wachtler, V. and Balasubramanian, M. (2003). Cytokinesis in fission yeast: a story of rings, rafts and walls. *Trends Genet.* **19**, 403-408.

Saito, T. T., Tougan, T., Kasama, T., Okuzaki, D. and Nojima, H. (2004). Mcp7, a meiosis-specific coiled-coil protein of fission yeast, associates with Meu13 and is required for meiotic recombination. *Nucleic Acids Res.* **32**, 3325-3339.

Sapperstein, S. K., Lupashin, V. V., Schmitt, H. D. and Waters, M. G. (1996). Assembly of the ER to Golgi SNARE complex requires Uso1p. *J. Cell Biol.* **132**, 755-767.

Scherthan, H. (2001). A bouquet makes ends meet. *Nat. Rev. Mol. Cell Biol.* **2**, 621-627.

Shimanuki, M., Miki, F., Ding, D. Q., Chikashige, Y., Hiraoka, Y., Horio, T. and Niwa, O. (1997). A novel fission yeast gene, *kms1*$^{+}$, is required for the formation of meiotic prophase-specific nuclear architecture. *Mol. Gen. Genet.* **254**, 238-249.

Shimada, M., Nabeshima, K., Tougan, T. and Nojima, H. (2002). The meiotic recombination checkpoint is regulated by checkpoint *rad*$^{+}$ genes in fission yeast. *EMBO J.* **21**, 2807-2818.

Sipiczki, M. and Ferenczy, L. (1977). Protoplast fusion of *Schizosaccharomyces pombe* auxotrophic mutants of identical mating-type. *Mol. Gen. Genet.* **151**, 77-81.

Svoboda, A., Bahler, J. and Kohli, J. (1995). Microtubule-driven nuclear movements and linear elements as meiosis-specific characteristics of the fission yeasts *Schizosaccharomyces versatilis* and *Schizosaccharomyces pombe*. *Chromosoma* **104**, 203-214.

Virgin, J. B. and Bailey, J. P. (1998). The M26 hotspot of *Schizosaccharomyces pombe* stimulates meiotic ectopic recombination and chromosomal rearrangements. *Genetics* **149**, 1191-1204.

Watanabe, T., Miyashita, K., Saito, T. T., Yoneki, T., Kakihara, Y., Nabeshima, K., Kishi, Y. A., Shimoda, C. and Nojima, H. (2001). Comprehensive isolation of meiosis-specific genes identifies novel proteins and unusual non-coding transcripts in *Schizosaccharomyces pombe*. *Nucleic Acids Res.* **29**, 2327-2337.

Yamamoto, A. and Hiraoka, Y. (2001). How do meiotic chromosomes meet their homologous partners?: lessons from fission yeast. *BioEssays* **23**, 526-533.

Yamamoto, A. and Hiraoka, Y. (2003). Cytoplasmic dynein in fungi: insights from nuclear migration. *J. Cell Sci.* **116**, 4501-4512.

Yamamoto, A., West, R. R., McIntosh, J. R. and Hiraoka, Y. (1999). A cytoplasmic dynein heavy chain is required for oscillatory nuclear movement of meiotic prophase and efficient meiotic recombination in fission yeast. *J. Cell Biol.* **145**, 1233-1249.

Yamamoto, A., Tsutsumi, C., Kojima, H., Oiwa, K. and Hiraoka, Y. (2001). Dynamic behavior of microtubules during dynein-dependent nuclear migrations of meiotic prophase in fission yeast. *Mol. Biol. Cell* **12**, 3933-3946.

Zickler, D. and Kleckner, N. (1999). Meiotic chromosomes: integrating structure and function. *Annu. Rev. Genet.* **33**, 603-754.

ELSEVIER

International Immunopharmacology 4 (2004) 119–126

International Immunopharmacology

www.elsevier.com/locate/intimp

Inhibitory effects of bucillamine on the expression of vascular cell adhesion molecule-1 in human umbilical vein endothelial cells

Hirotoshi Kikuchi, Kunio Isshi, Shunsei Hirohata*

Department of Internal Medicine, Teikyo University School of Medicine, 2-11-1 Kaga, Itabashi, Tokyo 173-8605, Japan

Received 4 July 2003; received in revised form 4 August 2003; accepted 13 November 2003

Abstract

Bucillamine (BUC) has been found to have beneficial effects in the treatment of rheumatoid arthritis (RA), in which the activation of endothelial cells plays an important role in the pathogenesis. The current studies examined the effect of BUC and its intramolecular disulfide form (BUC-ID) on the expression of adhesion molecules in human umbilical vein endothelial cells (HUVEC) stimulated with tumor necrosis factor-α (TNF-α). HUVEC (4×10^4/well) were incubated with medium M199 containing heparin and 20% FCS with endothelial cell growth supplement (ECGS) for 24 h in the presence or absence of BUC or BUC-ID, after which the culture medium was replaced with ECGS free medium. Then the cultures were further carried out for additional 24 h with TNF-α (10 ng/ml) in the presence or absence of BUC or BUC-ID. BUC-ID, but not BUC, appeared to suppress the expression of VCAM-1 on HUVEC stimulated with TNF-α in a dose-response manner at its pharmacologically relevant concentrations (0.3–3.0 μg/ml), whereas only the 3 μg/ml concentration level of BUC-ID had a statistically significant effect, although the effect was relatively small. By contrast, lower concentrations of BUC-ID (1–3 μg/ml) suppressed the secretion of soluble VCAM-1 by HUVEC much more effectively. Of note, at the concentration of 3 μg/ml neither BUC nor BUC-ID significantly influenced the expression of ICAM-1 and E-selectin on TNF-α stimulated HUVEC. These results indicate that BUC-ID, but not BUC, specifically downregulates the surface expression of VCAM-1 as well as the release of soluble VCAM-1 by HUVEC stimulated with TNF-α. BUC-ID suppressed the production of solubleVCAM-1 by RA bone marrow CD34+ cells stimulated with SCF, GM-CSF and TNF-α more effectively than BUC. The data thus suggest that one of the mechanisms of action of BUC involves the inhibition of the activation of endothelial cells.

Keywords: Rheumatoid arthritis; Bucillamine; Adhesion molecules; Endothelial cells; TNF-α; VCAM-1; ICAM-1; E-selectin

1. Introduction

Bucillamine [*N*-(2-mercapto-2-methylpropionyl)-L-cysteine] (BUC) is a disease-modifying antirheumatic drug [1]. The beneficial effects of BUC in the treatment of rheumatoid arthritis (RA) have been well appreciated in several clinical trials [1–3]. BUC is a thiol compound that differs from D-penicillamine (DP) by the presence of two free sulfhydryl groups. As a result, a considerable fraction of BUC can form an intramolecular disulfide (BUC-ID) that appears to have unique immunosuppressive activities [4]. Thus, BUC exerts immunosuppressive effects

* Correspondence author. Tel.: +81-3-3964-1211x1568; fax: +81-3-5375-1308.
E-mail address: shunsei@med.teikyo-u.ac.jp (S. Hirohata).

1567-5769/$ - see front matter © 2004 Elsevier B.V. All rights reserved.
doi:10.1016/j.intimp.2003.11.002

that are similar to those of DP, as well as unique inhibitory effects that depend upon the capacity of BUC to form an intramolecular disulfide, BUC-ID [4]. Moreover, we have also delineated that at pharmacologically attainable concentrations, BUC-ID directly suppresses B cell IgM production, but not T cell interferon-γ (IFN-γ) production, whereas DP inhibits the latter, but not the former, suggesting that as a result of the formation of the internal disulfide, BUC and DP have different targets of immunosuppressive action in vivo [5].

The hallmarks of the pathological changes in the RA synovium include hyperplasia of synovial lining cells and follicle-like aggregation of lymphocytes and plasma cells [6]. A number of studies have indicated that angiogenesis as well as activation of endothelial cells to express adhesion molecules plays a crucial role in recruiting inflammatory cells and immunocompetent cells into the synovium [7–9]. Of note, BUC has been shown to inhibit the production of vascular endothelial growth factor (VEGF), a potent inducer of angiogenesis, by cultured rheumatoid synovial cells [10] and bovine retinal microcapillary endothelial cells [11]. However, the effects of BUC and its metabolites on the expression of adhesion molecules in vascular endothelial cells have not yet been delineated. The current studies therefore examined the effects of BUC and BUC-ID on the expression of adhesion molecules in human umbilical vein endothelial cells (HUVEC) stimulated with TNF-α.

2. Materials and methods

2.1. Monoclonal antibodies (mAb) and reagents

A variety of mAb were used, including a murine IgG1 mAb directed at VCAM-1 (CD106) (clone 1G11; Immunotech, Marseille, France), a murine IgG1 mAb directed at ICAM-1 (CD54) (clone 84H10, Immunotech), a murine IgG1 mAb directed at E-selectin (CD62E) (clone 1.2B6, Southern Biotechnology Associates, Birmingham, AL) and a murine IgG1 control mAb (MOPC21) (Cappel Laboratories, West Chester, PA). TNF-α was purchased from PeproTech, London, UK. Bucillamine (BUC) and its intramolecular disulfide (BUC-ID) were synthesized and provided by Santen Pharmaceutical, Osaka, Japan.

2.2. Preparation of HUVEC cultures

HUVEC were isolated from single harvests in our laboratory as described [12]. HUVEC were maintained in M199 medium (Life Technologies, Grand Island, NY) supplemented with 20% FCS (Life Technologies), 100 μg/ml heparin, 50 μg/ml endothelial cell growth supplement (ECGS) (Becton Dickinson Labware, Bedford, MA), 2 mM L-glutamine, penicillin G (100 U/ml), streptomycin (100 μg/ml), and 25 mM HEPES (Life Technologies) in culture flasks coated with 20 μg/ml fibronectin (Ito ham, Tokyo, Japan). HUVEC were used at passages 3–5 for all the experiments.

2.3. Cell enzyme-linked immunosorbent assay (cell ELISA)

HUVEC (4×10^4/well) were incubated with medium M199 containing heparin and 20% FCS with ECGS in wells of 96-well flat bottom microtiter plates (No. 3596; Costar, Cambridge, MA) coated with fibronectin (20 μg/ml in PBS) for 24 h, after which the culture medium was replaced with ECGS free medium. Cultures were further carried out for additional 24 h with TNF-α (10 ng/ml). Various concentrations of BUC or BUC-ID were present throughout the total length of culture of 48 h. After the incubation, the wells were carefully aspirated and the cells were then fixed with 1% paraformaldehyde (PFA) for 5 min at 37 °C, followed by three times washes with PBS containing 0.05% Tween 20. After incubation with anti-VCAM-1, anti-ICAM-1, or anti-E-selectin (1 μg/ml) diluted in PBS containing 1% bovine serum albumin (Miles, Elkhart, IN) (PBS–BSA) for 1 h at 37 °C, the wells were washed with PBS-Tween 20 three times. Bound VCAM-1, ICAM-1, or E-selectin mAb were reacted with peroxidase conjugated $F(ab')_2$ fragments goat anti-mouse IgG (Cappel) diluted by 1:1000 in PBS–BSA for 1 h at 37 °C. Finally, the expression of VCAM-1, ICAM-1, or E-selectin was quantitated by the addition of peroxidase substrate solution containing 40 mg *o*-phenylenediamine and 10 μl 30% H_2O_2 in 100 ml 0.05 M citrate–phosphate buffer (pH 4.8). After incubation for 30 min at 37 °C, the reaction was stopped by addition of 5 N H_2SO_4,

and the absorbance of each well was measured at 492 nm, and the background at 630 nm was subtracted using a two-wave length microplate photometer (MTP-120, Corona Electric, Ibaraki, Japan). Within each experiment, each point was set in triplicate wells. At each point, mean ± S.D. of the triplicate wells was calculated.

2.4. Survival of HUVEC

Relative viable numbers of HUVEC was quantitated by MTT colorimetric assay after total length of cultures for 48 h. After 4 h of incubation with MTT, the reaction was stopped, and the absorbance at 570 nm was measured. Results were expressed as the mean ± S.D. of triplicate wells.

2.5. Preparation and culture of RA bone marrow CD34+ cells

Bone marrow samples were obtained from 2 patients with RA, who satisfied the American College of Rheumatology 1987 revised criteria for RA [13] and gave informed consent, during joint operations by intramedullary reaming via aspiration from a distal femoral canal prepared for implantation of an artificial femoral head. Mononuclear cells were isolated by centrifugation of heparinized bone marrow aspirates over sodium diatrizoate-Ficoll gradients (Histopaque; Sigma, St. Louis, MO). CD34+ cells were purified from the mononuclear cells by positive selection with magnetic beads (CD34 progenitor cell selection system; Dynal, Oslo, Norway). The cells thus prepared were >96% CD34+ cells and <0.5% CD19+ B cells, as previously described [14]. CD34+ cells were incubated in a 24-well microtiter plate with flat-bottomed wells (No. 3524; Costar) (10^5/well) with the presence of stem cell factor (SCF) (Pepro tech) (10 ng/ml), granulocyte macrophage-colony stimulating factor (GM-CSF) (Pepro Tech) (1 ng/ml) and tumor necrosis factor-α (TNF-α) (10 ng/ml). After 4 weeks of incubation, the culture supernatants were assayed for soluble VCAM-1.

2.6. Measurement of soluble VCAM-1

The concentrations of soluble VCAM-1 were analysed using an enzyme-linked immunosorbent assay (Cytoscreen™ Human sVCAM-1, Bio Source International, Camarillo, CA).

2.7. Statistical analysis

The significance of the effects of BUC and BUC-ID on HUVEC in each independent experiment was evaluated by Student's *t*-test. The significance of the effects of BUC-ID on the expression of VCAM-1 on HUVEC were further analysed in eight independent experiments by paired sample *t*-test.

3. Results

Initial experiments were carried out to explore the influences of pharmacologically relevant concentrations of BUC and BUC-ID on the proliferation and VCAM-1 expression of HUVEC. HUVEC were incubated with medium M199 containing heparin and 20% FCS with ECGS for 24 h, after which the culture medium was replaced with ECGS free medium. Cultures were further carried out for additional 24 h with the presence of TNF-α (10 ng/ml). Various concentrations of BUC or BUC-ID were present throughout the total length of cultures for 48 h. TNF-α increased the proliferation of HUVEC approximately twofold (OD 570: 0.144 ± 0.012 [mean ± S.D.] for medium alone vs. 0.230 ± 0.004 for TNF-α). As can be seen in Fig. 1, BUC and BUC-ID at any concentrations did not significantly influence the proliferation or viability of HUVEC. By contrast, BUC-ID, but not BUC, suppressed the expression of VCAM-1 on HUVEC stimulated with TNF-α in a dose-response manner (Fig. 2). To confirm the suppressive effect of BUC-ID on VCAM-1 expression on HUVEC, eight different experiments were carried out using different sources of HUVEC. As can be seen in Fig. 3, BUC-ID at 3.0 μg/ml (approximately 1.5×10^{-5} M) significantly suppressed the expression of VCAM-1 on TNF-α stimulated HUVEC in these eight different experiments, although the suppressive effects were relatively small (15–20% inhibition). These results indicate that at pharmacologically relevant concentrations BUC-ID suppresses the expression of VCAM-1 without affecting the proliferation of HUVEC, whereas BUC itself does not display any significant influences on the proliferation or VCAM-1 expression on HUVEC.

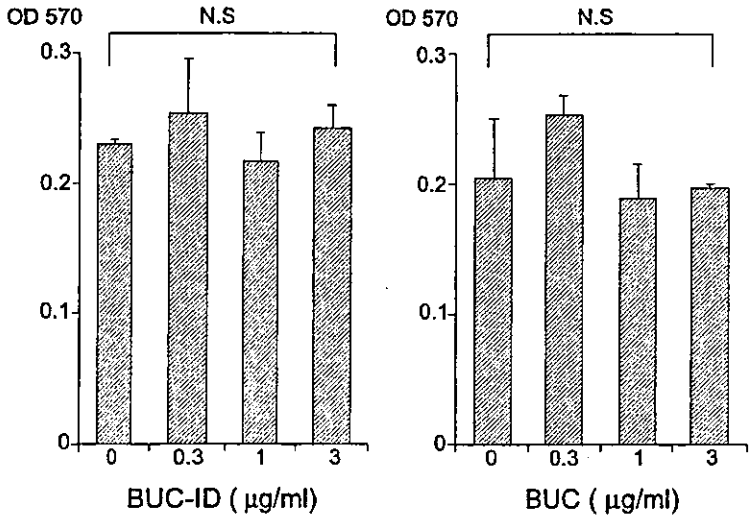

Fig. 1. Effect of BUC and BUC-ID on the proliferation of HUVEC. HUVEC (4×10^4/well) were incubated with medium M199 containing heparin and 20% FCS with endothelial cell growth supplement (ECGS) for 24 h, after which the culture medium was replaced with ECGS free medium. Cultures were further carried out for additional 24 h with TNF-α (10 ng/ml). Various concentrations of BUC or BUC-ID were present throughout the total length of cultures as indicated. After the incubation, the proliferation of HUVEC was assessed by MTT colorimetric assay. Statistical analysis was carried out by Student's *t*-test. Representative of eight independent experiments.

Previous studies suggested that the expression of VCAM-1 might be regulated with different mechanisms from that of ICAM-1 and E-selectin [12,15]. Next experiments therefore compared the influences of BUC and BUC-ID on the expression of VCAM-1, ICAM-1, and E-selectin. As can be seen in Table 1, at

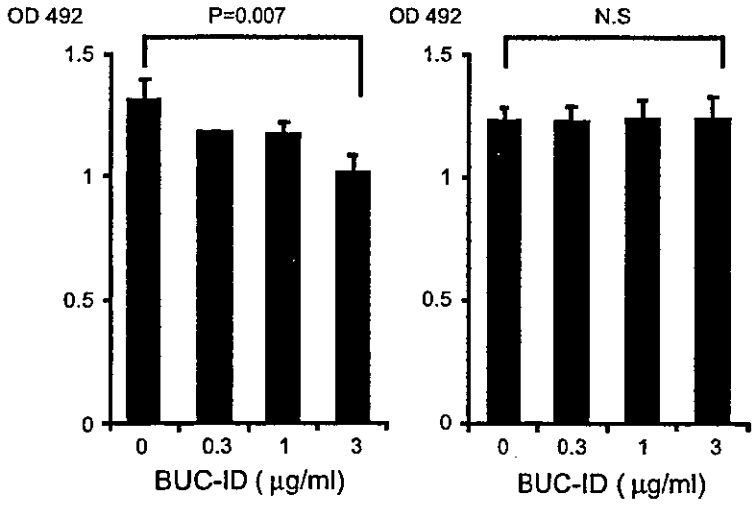

Fig. 2. Effect of BUC and BUC-ID on the expression of VCAM-1 on HUVEC. HUVEC (4×10^4/well) were incubated with medium M199 containing heparin and 20% FCS with endothelial cell growth supplement (ECGS) for 24 h, after which the culture medium was replaced with ECGS free medium. Cultures were further carried out for additional 24 h with TNF-α (10 ng/ml). Various concentrations of BUC or BUC-ID were present throughout the total length of cultures as indicated. After the incubation, the expression of VCAM-1 on HUVEC was assessed by cell ELISA. Statistical analysis was carried out by Student's *t*-test. Representative of eight independent experiments.

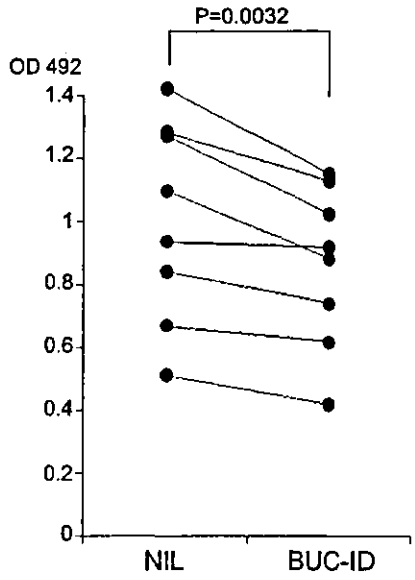

Fig. 3. Effect of BUC-ID on the expression of VCAM-1 on HUVEC. HUVEC (4×10^4/well) were incubated with medium M199 containing heparin and 20% FCS with endothelial cell growth supplement (ECGS) for 24 h, after which the culture medium was replaced with ECGS free medium. Cultures were further carried out for additional 24 h with TNF-α (10 ng/ml). BUC-ID (3 μg/ml) was present throughout the total length of cultures as indicated. After the incubation, the expression of VCAM-1 on HUVEC was assessed by cell ELISA. Statistical analysis was carried out by paired sample *t*-test.

a concentration of 3 μg/ml (approximately 1.5×10^{-5} M) BUC-ID, but not BUC, significantly suppressed the expression of VCAM-1 on HUVEC. By contrast, either BUC or BUC-ID did not significantly influence the expression of ICAM-1 or E-selectin on HUVEC stimulated with TNF-α. These results confirm that the expression of VCAM-1 on HUVEC is regulated by different mechanisms from that of ICAM-1 and E-selectin. Moreover, the data indicate that the suppressive effect of BUC-ID is specific for VCAM-1 in HUVEC.

A number of studies have suggested that soluble VCAM-1 (sVCAM-1) is generated through cleavage of membrane bound VCAM-1 by proteolytic enzyme [16,17]. It was thus possible that the down-regulation of the expression of VCAM-1 on HUVEC by BUC-ID might be a result of increased cleavages of VCAM-1. To test this possibility, the next experiment examined the effects of BUC-ID on the production of sVCAM-1 by HUVEC stimulated with TNF-α. As shown in Fig. 4, BUC-ID also suppressed the production of sVCAM-1 by HUVEC stimulated with TNF-α. Of note, the inhibitory effects of BUC-ID on the production of sVCAM-1 were much more striking than those on the surface expression of VCAM-1. The data therefore indicate that BUC-ID inhibits the synthesis of VCAM-1, leading to the decreased expression of VCAM-1 on the surface of HUVEC as well as the decreased release of sVCAM-1.

It has been recently shown that RA bone marrow CD34+ cells have enhanced capacities to induce activation of endothelial cells to express adhesion molecules, such as VCAM-1 [18]. Final experiments were thus designed to examine the effects of BUC-ID and BUC on the production of sVCAM-1 by RA bone marrow CD34+ cells stimulated with SCF, GM-CSF and TNF-α for 4 weeks. As shown in Fig. 5, BUC-ID (0.66 μg/ml) as well as BUC (3 μg/ml) suppressed the production of sVCAM-1. It should be noted that BUC-ID at the lower concentration (0.66 μg/ml) displayed more striking suppressive effects than BUC at the higher concentration (3 μg/ml). The results strongly suggest that BUC-ID might suppress the activation of endothelial cells in RA the way it works in HUVEC.

Table 1
Differential effects of BUC-ID on the TNF-α induced expression of various adhesion molecules on HUVEC

Inhibitors	Expression of adhesion molecules (OD492)		
	VCAM-1	ICAM-1	E-selectin
Nil	1.232 ± 0.046	2.263 ± 0.033	0.471 ± 0.040
BUC	1.238 ± 0.087	2.399 ± 0.044	0.511 ± 0.016
BUC-ID	1.023 ± 0.067*	2.091 ± 0.152	0.487 ± 0.011

HUVEC (4×10^4/well) were incubated with medium M199 containing heparin and 20% FCS with endothelial cell growth supplement (ECGS) for 24 h, after which the culture medium was replaced with ECGS free medium. HUVEC were stimulated with TNF-α (10 ng/ml) for 3 (E-selection) or 24 h (VCAM-1, ICAM-1). Either BUC (3.0 μg/ml) or BUC-ID (3.0 μg/ml) was present throughout the total length of cultures. After the incubation, the expression of various adhesion molecules was assessed by cell ELISA. Data are expressed mean ± S.D. of triplicate determinations. Statistical analysis was carried out by Student's *t*-test. Representative of two independent experiments.

* Significantly suppressed compared with medium alone (Nil) at $p < 0.05$.

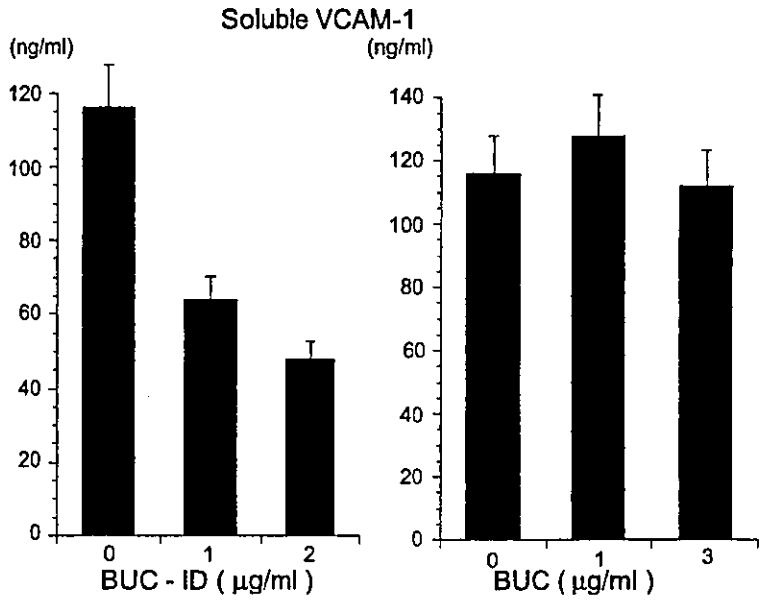

Fig. 4. Effect of BUC and BUC-ID on the production of soluble VCAM-1 by HUVEC. HUVEC (4×10^4/well) were incubated with medium M199 containing heparin and 20% FCS with endothelial cell growth supplement (ECGS) for 24 h, after which the culture medium was replaced with ECGS free medium. Cultures were further carried out for additional 24 h with TNF-α (10 ng/ml). Various concentrations of BUC or BUC-ID were present throughout the total length of cultures as indicated. After the incubation, the culture supernatants were harvested and the concentration of soluble VCAM-1 was measured by ELISA. Representative of two independent experiments.

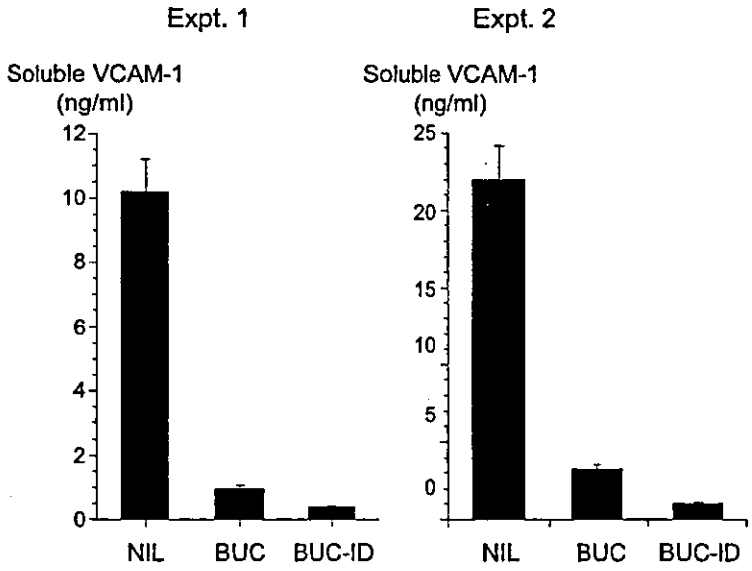

Fig. 5. Effect of BUC and BUC-ID on the production of soluble VCAM-1 by RA bone marrow CD34+ cells. RA bone marrow CD34+ cells were cultured in the presence of SCF (10 ng/ml), GM-CSF (1 ng/ml) and TNF-α (10 ng/ml) with or without BUC (3 μg/ml) or BUC-ID (0.66 μg/ml). After 4 weeks of incubation, the culture supernatants were harvested and the concentration of soluble VCAM-1 was measure by ELISA.

4. Discussion

The results in the present study have demonstrated that BUC-ID, an intramolecular disulfide form of BUC, inhibits the expression of VCAM-1 on HUVEC at its pharmacologically relevant concentrations, although the suppressive effects were relatively small. Thus, BUC-ID significantly suppressed the expression of VCAM-1 on HUVEC at the concentration of 3 μg/ml. Although the plasma concentrations of BUC-ID and BUC have been shown to reach 2.0 μg/ml in normal individuals [19], no data are available in RA patients. Since the plasma concentrations of a similar compound D-penicillamine have been shown to be 1–3 μg/ml in RA patients [20], it is conceivable that BUC-ID might reach 3 μg/ml in RA patients. Since BUC-ID did not suppress the proliferative response of HUVEC, it is clear that its inhibitory effects on VCAM-1 expression are not due to suppression of cell growth or induction of apoptosis. In addition, BUC-ID also suppressed the production of sVCAM-1 by HUVEC, obviating the possibility that BUC-ID might promote the proteolytic cleavage of VCAM-1 expressed on the surface of HUVEC. The data therefore strongly suggest that BUC-ID might inhibit de novo synthesis of VCAM-1 in HUVEC. Of interest, BUC itself did not display the capacity to inhibit the expression of VCAM-1 on HUVEC. In this regard, the differential action of BUC and BUC-ID on HUVEC is comparable to that on human B cells. Thus, BUC-ID suppressed the production of IgM much more effectively than BUC at pharmacologically relevant concentrations [4]. It is therefore suggested that BUC-ID might play more important roles than BUC itself in the expression of antirheumatic effects of BUC in RA patients.

The hallmarks of the pathological changes in the RA synovium include hyperplasia of synovial lining cells and follicle-like aggregation of lymphocytes and plasma cells [6]. A number of studies have demonstrated that angiogenesis as well as activation of endothelial cells plays a crucial role in recruiting lymphocytes and monocyte-lineage cells [7–9]. In fact, therapeutic intervention of angiogenesis, such as angiostatin, has been shown to inhibit the development of murine type II collagen arthritis [21]. Moreover, several disease-modifying anti-rheumatic drugs have been found to suppress the production of angiogenic factors by synovial cells [10,22]. Thus, BUC suppressed the production of VEGF by cultured synovial cells as well as decreased the serum VEGF concentrations in RA patients [22]. In addition to the inhibitory effects of BUC in VEGF production, the results in the current studies have demonstrated that BUC-ID suppresses VCAM-1 expression on HUVEC. It is therefore suggested that these effects of BUC and BUC-ID on angiogenesis and endothelial cell activation might also account at least in part for the antirheumatic effects of BUC, in addition to their effects on immunocompetent cells, such as B cells and T cells [4,5].

Of note, the inhibitory effects of BUC-ID on the secretion of sVCAM-1 by HUVEC were much more striking than those on the surface expression of VCAM-1. It has been recently disclosed that tumor necrosis factor-α-converting enzyme (TACE) plays a pivotal role in the shedding of VCAM-1 [23]. It is therefore possible that BUC-ID might also inhibit the activity and/or the expression of TACE. Since previous studies suggested that TACE might also be involved in the pathogenesis of RA synovitis [24], further studies to delineate the effects of BUC-ID on TACE would be important for a complete understanding of the mechanism of action of BUC in RA.

The results in the present study also disclosed that BUC-ID also suppressed the production of sVCAM-1 by RA bone marrow CD34+ cells stimulated with SCF, GM-CSF and TNF-α, much more effectively than BUC. It has been shown that bone marrow CD34+ progenitor cells contain progenitors of endothelial cells that respond to SCF and GM-CSF [25]. It is therefore likely that BUC-ID might suppress the activation of endothelial cells in RA the way it works in HUVEC, although it is also possible that BUC-ID might inhibit the development of endothelial cells from RA bone marrow CD34+ cells.

Acknowledgements

This work is supported by a grant from Santen Pharmaceutical, Osaka, Japan.

References

[1] Shiokawa Y, Abe C, Warabi S, Abe H, Kageyama T, et al. Clinical evaluation of SA96 on rheumatoid arthritis (in Japanese). Jpn J Inflamm 1985;5:333–43.

[2] Abe C. Clinical evaluation of immunomodulators. Int J Immunother 1985;1:7–10.
[3] Kashiwazaki S, Shiokawa Y. Bucillamine: a new immunomodulator. Int J Immunother 1987;3:1–6.
[4] Hirohata S, Lipsky PE. Regulation of B cell function by bucillamine, a novel disease-modifying antirheumatic drug. Clin Immunol Immunopathol 1993;66:43–51.
[5] Hirohata S, Lipsky PE. Comparative inhibitory effects of bucillamine and D-penicillamine on the function of human B cells and T cells. Arthritis Rheum 1994;37:942–50.
[6] Schumacher Jr. HR, Bautista BB, Krauser RE, Mathur AK, Gall EP. Histological appearance of the synovium in early rheumatoid arthritis. Semin Arthritis Rheum 1994;23(Suppl. 2):3–10.
[7] Koch AE. Angiogenesis: implications for rheumatoid arthritis. Arthritis Rheum 1998;41:951–62.
[8] Cronstein BN, Weissmann G. The adhesion molecules of inflammation. Arthritis Rheum 1993;36:147–57.
[9] Springer TA. Traffic signals for lymphocyte recirculation and leukocyte emigration: the multistep paradigm. Cell 1994;76:301–14.
[10] Nagashima M, Yoshino S, Aono H, Takai M, Sasano M. Inhibitory effects of anti-rheumatic drugs on vascular endothelial growth factor in cultured rheumatoid synovial cells. Clin Exp Immunol 1999;116:360–5.
[11] Koyama S, Takagi H, Otani A, Oh H, Nishimura K, Honda Y. Inhibitory mechanism of vascular endothelial growth factor (VEGF) by bucillamine. Br J Pharmacol 2002;137:901–9.
[12] Marui N, Offermann MK, Swerlick R, Kunsch C, Rosen CA, et al. Vascular cell adhesion molecule-1 (VCAM-1) gene transcription and expression are regulated through an antioxidant-sensitive mechanism in human vascular endothelial cells. J Clin Invest 1993;92:1866–74.
[13] Arnett FC, Edworthy SM, Bloch DA, McShane DJ, Fries JF, et al. The American Rheumatism Association 1987 revised criteria for the classification of rheumatoid arthritis. Arthritis Rheum 1998;31:315–24.
[14] Ueda T, Tsuji K, Yoshio H, Ebihara Y, Yagasaki H, et al. Expansion of human NOD/SCID-repopulating cells by stem cell factor, Flk2/Flt3 ligand, thrombopoietin, IL-6, and soluble IL-6 receptor. J Clin Invest 2000;105:1013–21.
[15] Gille J, Paxton LL, Lawley TJ, Caughman SW, Swerlick RA. Retinoic acid inhibits the regulated expression of vascular cell adhesion molecule-1 by cultured dermal microvascular endothelial cells. J Clin Invest 1997;99:492–500.
[16] Gearing AJH, Hemingway I, Pigott R, Hughes J, Rees AJ, Cashman SJ. Soluble forms of vascular adhesion molecules, E-selectin, ICAM-1 and VCAM-1: pathological significance. Ann N Y Acad Sci 1992;667:324–31.
[17] Gearing AJH, Newman W. Circulating adhesion molecules in disease. Immunol Today 1993;14:506–12.
[18] Hirohata S, Yanagida T, Nampei A, Hashimoto H, Yoshikawa H, et al. Enhanced generation of VEGF and soluble VCAM-1 from CD34+ progenitor cells of the bone marrow in rheumatoid arthritis. Arthritis Rheum 2003;48:S341 [Suppl.].
[19] Eguchi K, Kawakami A, Ida H, Nakashima M, Yamashita I, et al. Bucillamine inhibits T cell adhesion to human endothelial cells. J Rheumatol 1992;119:1045–50.
[20] Seideman P, Lindström B. Phamacokinetic interactions of penicillamine in rheumatoid arthritis. J Rheumatol 1989;16:473–4.
[21] Kim JM, Ho SH, Park EJ, Hahn W, Cho H, et al. Angiostatin gene transfer as an effective treatment strategy in murine collagen-induced arthritis. Arthritis Rheum 2002;46:793–801.
[22] Nagashima M, Wauke K, Hirano D, Ishigami S, Aono H, et al. Effects of combinations of anti-rheumatic drugs on the production of vascular endothelial growth factor and basic fibroblast growth factor in cultured synoviocytes and patients with rheumatoid arthritis. Rheumatology 2000;39:1255–62.
[23] Garton KJ, Gough PJ, Philalay J, Wille PT, Blobel CP, et al. Stimulated shedding of vascular cell adhesion molecule 1 (VCAM-1) is mediated by tumor necrosis factor-α-converting enzyme (ADAM 17). J Biol Chem 2003;278:37459–64.
[24] Ohta S, Harigai M, Tanaka M, Kawaguchi Y, Sugiura T, et al. Tumor necrosis factor-alpha (TNF-alpha) converting enzyme contributes to production of TNF-alpha in synovial tissues from patients with rheumatoid arthritis. J Rheumatol 2001;28:1756–63.
[25] Pelletier L, Regnard J, Fellmann D, Charbord P. An in vitro model for the study of human bone marrow angiogenesis: role of hematopoietic cytokines. Lab Invest 2000;80:501–11.

ARTHRITIS & RHEUMATISM
Vol. 50, No. 12, December 2004, pp 3888–3896
DOI 10.1002/art.20729

Enhanced Generation of Endothelial Cells From CD34+ Cells of the Bone Marrow in Rheumatoid Arthritis

Possible Role in Synovial Neovascularization

Shunsei Hirohata,[1] Tamiko Yanagida,[1] Akihide Nampei,[2] Yasuo Kunugiza,[2] Hideo Hashimoto,[2] Tetsuya Tomita,[2] Hideki Yoshikawa,[2] and Takahiro Ochi[3]

Objective. **To examine the capacity of bone marrow CD34+ cells to generate endothelial cells, in order to assess the role of bone marrow in neovascularization in the synovium of rheumatoid arthritis (RA).**

Methods. **CD34+ cells purified from the bone marrow of 13 patients with active RA and 9 control subjects (7 osteoarthritis [OA] patients and 2 healthy individuals) were cultured in the presence of stem cell factor (10 ng/ml) and granulocyte–macrophage colony-stimulating factor (1 ng/ml). After 18 days of incubation, the generation of endothelial cells was assessed by flow cytometry. The generation of endothelial cells was compared with the degree of vascularization in the synovial tissues and with the microvessel densities in the synovium, as determined by microscopy. The expression of vascular endothelial growth factor receptor 2/kinase insert domain receptor (KDR) messenger RNA (mRNA) in CD34+ cells was examined by quantitative reverse transcription–polymerase chain reaction.**

Results. **The generation of CD14+ cells from bone marrow–derived CD34+ cells from RA patients was comparable to that from control subjects. However, the generation of von Willebrand factor (vWF)–positive cells and CD31+/vWF+ cells from RA bone marrow–derived CD34+ cells was significantly higher than that from control subjects ($P = 0.004$ and $P = 0.030$, respectively). The generation of vWF+ cells from bone marrow CD34+ cells correlated significantly with the microvessel densities in the synovial tissues ($r = 0.569$, $P = 0.021$). Finally, RA bone marrow CD34+ cells expressed KDR mRNA at higher levels than OA bone marrow CD34+ cells.**

Conclusion. **These results indicate that RA bone marrow CD34+ cells have enhanced capacities to differentiate into endothelial cells in relation to synovial vascularization. The data therefore suggest that bone marrow CD34+ cells might contribute to synovial neovascularization by supplying endothelial precursor cells and, thus, play an important role in the pathogenesis of RA.**

Rheumatoid arthritis (RA) is a chronic inflammatory disease characterized by hyperplasia of synovial lining cells (1). Synovial lining cells consist of type A (macrophage-like) synoviocytes and type B (fibroblast-like) synoviocytes. Recent studies have suggested that type A synoviocytes are derived from monocyte precursors in the bone marrow (2). Accordingly, it has been shown that the spontaneous generation of CD14+ cells from bone marrow–derived CD14− progenitor cells is accelerated in RA, resulting in the facilitated entry of such CD14+ cells into the synovium (3). On the other hand, type B synoviocytes have a morphologic appearance of fibroblasts as well as the capacity to produce and secrete a variety of factors, including proteoglycans, cytokines, arachidonic acid metabolites, and matrix met-

Supported by a grant from the Ministry of Health, Labor, and Welfare of Japan.

[1]Shunsei Hirohata, MD, Tamiko Yanagida, PhD: Teikyo University School of Medicine, Tokyo, Japan; [2]Akihide Nampei, MD, PhD, Yasuo Kunugiza, MD, PhD, Hideo Hashimoto, MD, PhD, Tetsuya Tomita, MD, PhD, Hideki Yoshikawa, MD: Osaka University Medical School, Osaka, Japan; [3]Takahiro Ochi, MD: Sagamihara National Hospital, Kanagawa, Japan.

Address correspondence and reprint requests to Shunsei Hirohata, MD, Department of Internal Medicine, Teikyo University School of Medicine, 2-11-1 Kaga, Itabashi-ku, Tokyo 173-8605, Japan. E-mail: shunsei@med.teikyo-u.ac.jp.

Submitted for publication February 19, 2004; accepted in revised form September 2, 2004.

alloproteinases (MMPs), that lead to the destruction of joints (4). Whereas type B synoviocytes are thought to arise from the sublining tissue or other support structures of the joint (4), recent studies have suggested that they are also derived from bone marrow progenitor cells (5). Increasing attention has therefore been given to the role of the bone marrow in the pathogenesis of RA (6).

In the RA joint, the massive proliferating synovium forms an invading tissue called pannus, which results in the destruction of cartilage and bone. A number of studies have shown that persistent neovascularization is a crucial support to the continuous proliferation of the synovium, through delivery of nutrients and recruitment of inflammatory cells into the synovium (7,8). It was a long-held belief that vessels in the embryo developed from endothelial progenitors (vasculogenesis), whereas spouting of vessels in the adult resulted only from division of differentiated endothelial cells (angiogenesis) (9). Thus, the neovascularization in RA synovium has been attributed to angiogenesis, a process characterized by spouting of new capillaries from preexisting blood vessels (10).

Asahara et al (11), however, isolated endothelial progenitor cells from adult human peripheral blood using magnetic bead selection of CD34+ hematopoietic cells, and thus demonstrated that human peripheral blood CD34+ cells differentiated in vitro into endothelial cells, which expressed endothelial markers, including CD31. In addition, those investigators found that human CD34+ cells were incorporated into neovascularized hind limb ischemic sites in animal models (11). Since the time these observations were reported, it has also been found that endothelial progenitor cells capable of contributing to capillary formation can be derived from the bone marrow, possibly playing a role in the de novo formation of capillaries without preexisting blood vessels (12–14). Thus, the accumulating evidence has suggested that bone marrow–derived endothelial cells might be involved in several disorders characterized by excessive angiogenesis, such as myocardial infarction (15). However, the role of bone marrow in RA synovial neovascularization has not been explored.

It has been demonstrated that early endothelial progenitor cells in bone marrow express CD34, CD133, and vascular endothelial growth factor receptor 2 (VEGFR-2)/kinase insert domain receptor (KDR) (15). In general, early endothelial progenitor cells in the bone marrow are positive for CD34/CD133/VEGFR-2, whereas circulating endothelial progenitor cells are positive for CD34/VEGFR-2/CD31, negative for CD133, and are beginning to express von Willebrand factor (vWF) (15). Thus, it appears that vWF is expressed on fully matured endothelial cells.

The current studies were undertaken to explore whether CD34+ cells derived from the bone marrow of RA patients might have an enhanced capacity to generate endothelial cells so that we could assess the role of the bone marrow in the neovascularization of RA synovium. The results clearly indicate that bone marrow–derived CD34+ cells from RA patients differentiate into vWF+ endothelial cells upon stimulation with stem cell factor (SCF) and granulocyte–macrophage colony-stimulating factor (GM-CSF) much more effectively than do those from control subjects. The data therefore suggest that bone marrow CD34+ cells might play a role in the synovial hyperplasia in RA through mobilization of endothelial progenitor cells into the synovium, where angiogenesis is activated.

MATERIALS AND METHODS

Patients and samples. Bone marrow samples from 13 RA patients (1 man and 12 women; mean age 58.2 years [age range 45–72 years]) were obtained during joint operation through aspiration from the iliac crest. All RA patients met the American College of Rheumatology (formerly, the American Rheumatism Association) 1987 revised criteria (16). As controls, bone marrow samples were similarly obtained from 7 patients with osteoarthritis (OA) (7 women; mean age 70.6 years [age range 67–74]). All study patients gave their informed consent for study. In addition, bone marrow–derived CD34+ cells from 2 healthy individuals (2 men; ages 27 years and 24 years) were purchased from BioWhittaker (Walkersville, MD). Synovial tissues were also obtained from 10 of the RA patients and 6 of the OA patients during the same joint operation.

A second group of bone marrow samples was obtained from an additional 10 RA patients (3 men and 7 women; mean age 62.6 years) and an additional 4 OA patients (2 men and 2 women; mean age 72.6 years). These bone marrow samples were used in analyses of the expression of KDR messenger RNA (mRNA). These patients also gave their informed consent for study. In addition, samples from 7 of the RA patients and 6 of the OA patients from the first group described above were included in the study of KDR mRNA expression.

Culture medium and reagents. RPMI 1640 medium (Life Technologies, Grand Island, NY) supplemented with penicillin G (100 units/ml), streptomycin (100 μg/ml), L-glutamine (0.3 mg/ml), and 10% fetal bovine serum (Life Technologies) was used for all cultures. Recombinant human GM-CSF and SCF were purchased from PeproTech (London, UK).

Preparation and culture of bone marrow–derived CD34+ cells. Mononuclear cells were isolated by centrifugation of heparinized bone marrow aspirates over sodium

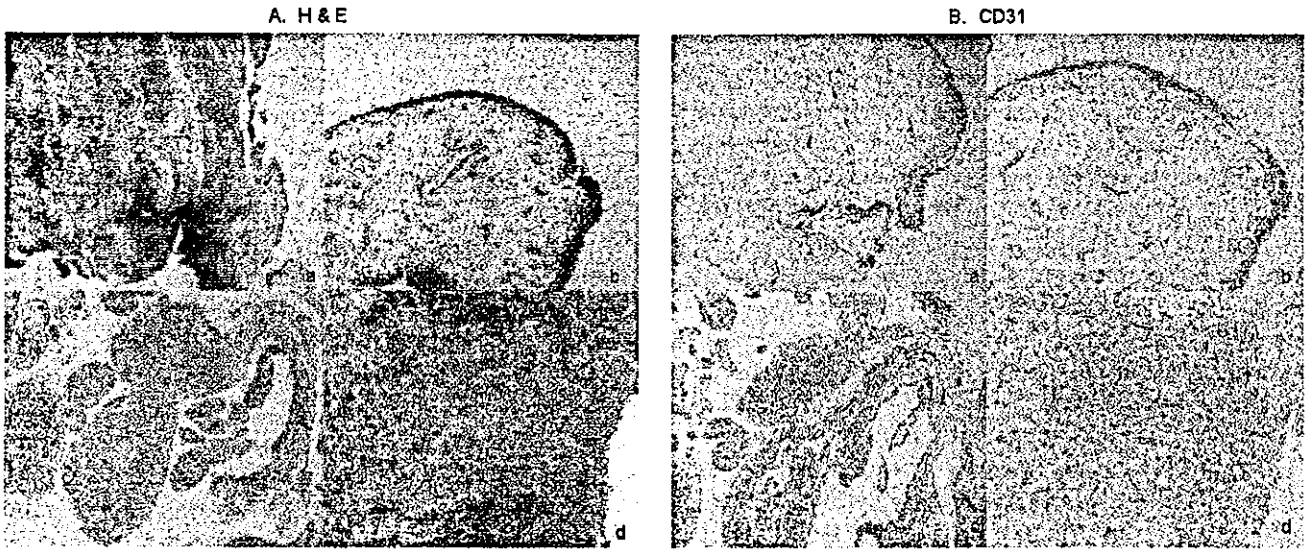

Figure 1. Histologic features (A) and immunohistochemistry of CD31 cells (B) in the synovium of patients with osteoarthritis (OA) and rheumatoid arthritis (RA). Four representative samples of synovium from OA (a and b) and RA (c and d) patients are presented, showing trace (a), mild (b), moderate (c), and strong (d) neovascularization. H&E = hematoxylin and eosin. (Original magnification × 25.)

diatrizoate-Ficoll gradients (Histopaque; Sigma, St. Louis, MO). CD34+ cells were purified from the mononuclear cells through positive selection using magnetic beads (Dynal CD34 progenitor cell selection system; Dynal, Oslo, Norway). CD34+ cells thus prepared were ~95% CD34+ cells and <0.5% CD19+ B cells, as previously described (5).

CD34+ cells were incubated in a 24-well microtiter plate with flat-bottomed wells (no. 3524; Costar, Cambridge, MA) at a density of 1.0×10^5/well in the presence of SCF (10 ng/ml) and GM-CSF (1 ng/ml). After 18 days of incubation, the cells were stained with various antibodies and analyzed by flow cytometry.

Immunofluorescence staining and analysis. Cultured CD34+ cells were stained with saturating concentrations of antibodies, including fluorescein isothiocyanate (FITC)–conjugated anti–HLA-DR monoclonal antibody (mAb) (mouse IgG2b; Immunotech, Marseilles, France), FITC-conjugated sheep anti-vWF IgG (Cosmo Bio, Tokyo, Japan), phycoerythrin (PE)–conjugated anti-CD14 mAb (mouse IgG2a; Immunotech), PE-conjugated anti-CD31 mAb (mouse IgG1; Immunotech), PE-conjugated murine IgG1 and IgG2a control mAb or FITC-conjugated murine IgG2b control mAb, which were raised against *Aspergillus niger* glucose oxide, an enzyme that is neither present nor inducible in mammalian tissues (Dako, Glostrup, Denmark), or FITC-conjugated control sheep IgG purified from normal sheep serum (Rockland, Gilbertsville, PA).

Briefly, the cells were washed with 2% normal human serum in phosphate buffered saline (PBS), pH 7.2, and 0.1% sodium azide (staining buffer), and the cells were stained with saturating concentrations of a variety of antibodies at 4°C for 30 minutes. The cells were then washed 3 times with staining buffer and fixed with 1% paraformaldehyde in PBS for at least 5 minutes at room temperature. Cells were analyzed using an Epics XL flow cytometer (Coulter, Hialeah, FL) equipped with an argon-ion laser at 488 nm. A combination of low-angle and 90° light scatter measurements (forward scatter versus side scatter) was used to identify bone marrow cells. The percentages of cells that stained positive for each mAb were determined by integration of cells above a specified fluorescence channel, which was calculated in relation to an isotype-matched control mAb.

Synovial histopathology and determination of microvessel densities. Synovial tissues were fixed in formalin, embedded in paraffin, and stained with hematoxylin and eosin. To visualize endothelial cells in the synovium, the paraffin-embedded sections were also stained with murine anti-CD31 mAb (clone JC/70A; Dako) and then developed using a Dako Envision kit, which includes horseradish peroxidase and diaminobenzidine. The degree of neovascularization was analyzed under light microscopy and scored as 0 (trace), 1 (mild), 2 (moderate), or 3 (strong) (Figures 1A and B). Grades were assigned by 2 independent observers (SH and TY) who had no knowledge of the diagnosis of the patients from whom the tissues had been obtained. When grades differed (2 of 16 cases), the synovium was reexamined, and a consensus was reached.

Sections were photographed with an Olympus DP11 digital camera (Olympus, Tokyo, Japan), and the CD31+ microvessel densities were determined by counting the vascular structures with a clearly defined lumen or linear shape as seen on the photographs. The final microvessel density was calculated as the mean score of the 3 1-mm^2 fields with the highest individual scores (17).

Measurement of cytokines in the culture supernatants. Concentrations of tumor necrosis factor α (TNFα) and vascular endothelial growth factor (VEGF) in the culture supernatants were measured by enzyme-linked immunosorbent assay